TITLE: Fibroblast-expressed LRRC15 suppresses SARS-CoV-2 infection and controls antiviral and antifibrotic transcriptional programs.

Authors

Lipin Loo[1,11], Matthew A. Waller[1,11], Cesar L. Moreno[1], Alexander J. Cole[2], Alberto Ospina Stella[3], Oltin-Tiberiu Pop[4], Ann-Kristin Jochum[4,5], Omar Hasan Ali[4,6,7], Christopher E. Denes[1], Zina Hamoudi[1], Felicity Chung[1], Anupriya Aggarwal[3], Jason K. K. Low[8], Karishma Patel[8], Rezwan Siddiquee[8], Taeyoung Kang[9], Suresh Mathivanan[9], Joel P. Mackay[8], Lukas Flatz[4,10], Daniel Hesselson[2], Stuart Turville[3], G. Gregory Neely[1,12]

Affiliations

[1]Charles Perkins Centre, Dr. John and Anne Chong Lab for Functional Genomics, Centenary Institute, and School of Life and Environmental Sciences, University of Sydney, Camperdown, NSW, Australia.

[2]Centenary Institute and Faculty of Medicine and Health, The University of Sydney, Sydney, NSW, 2006, Australia

[3]The Kirby Institute, University of New South Wales, New South Wales, Australia.

[4]Institute for Immunobiology, Kantonsspital St. Gallen, St. Gallen, Switzerland

[5]Institute for Pathology, Kantonsspital St. Gallen, St. Gallen, Switzerland

[6]Department of Medical Genetics, Life Sciences Institute, University of British Columbia, Vancouver, British Columbia, Canada.

22 [7]Department of Dermatology, University Hospital Zurich, University of Zurich, Zurich,
23 Switzerland.

24 [8]School of Life and Environmental Sciences, The University of Sydney, Sydney, New South
25 Wales 2006, Australia.

26 [9]Department of Biochemistry and Genetics, La Trobe Institute for Molecular Science, La Trobe
27 University, Melbourne, VIC, Australia.

28 [10]Center for Dermatooncology, Department of Dermatology, Eberhard Karls University of
29 Tübingen, Tübingen, Germany

30 [11]These authors contributed equally

31 [12]Lead contact

32 *Correspondence: greg.neely@sydney.edu.au (G.G.N.)

33

Abstract

Although ACE2 is the primary receptor for SARS-CoV-2 infection, a systematic assessment of host factors that regulate binding to SARS-CoV-2 spike protein has not been described. Here we use whole genome CRISPR activation to identify host factors controlling cellular interactions with SARS-CoV-2. Our top hit was a *TLR*-related cell surface receptor called *leucine-rich repeat-containing protein 15* (*LRRC15*). *LRRC15* expression was sufficient to promote SARS-CoV-2 Spike binding where they form a cell surface complex. *LRRC15* mRNA is expressed in human collagen-producing lung myofibroblasts and LRRC15 protein is induced in severe COVID-19 infection where it can be found lining the airways. Mechanistically, LRRC15 does not itself support SARS-CoV-2 infection, but fibroblasts expressing LRRC15 can suppress both pseudotyped and authentic SARS-CoV-2 infection in *trans*. Moreover, LRRC15 expression in fibroblasts suppresses collagen production and promotes expression of IFIT, OAS, and MX-family antiviral factors. Overall, LRRC15 is a novel SARS-CoV-2 spike-binding receptor that can help control viral load and regulate antiviral and antifibrotic transcriptional programs in the context of COVID-19 infection.

Keywords

host defense, LRRC15, SARS-CoV-2, COVID-19, Spike, CRISPR activation screen, fibrosis, antiviral response

54 **Introduction**

55

56 The Coronavirus 2019 (COVID-19) pandemic, caused by SARS-CoV-2, represents the greatest
57 public health challenge of our time. As of October 2022, there have been over 620,000,000
58 reported cases of COVID-19 globally and more than 6,500,000 deaths (WHO). SARS-CoV-2
59 shows high sequence similarity (79.6%) with severe acute respiratory syndrome coronavirus
60 (SARS-CoV-1), and because of this similarity, angiotensin-converting enzyme 2 (ACE2), the
61 primary entry receptor for SARS-CoV-1, was quickly identified as the SARS-CoV-2 Spike
62 receptor[1–4]. However, a comprehensive search for other host factors that promote SARS-CoV-2
63 Spike binding has not yet been reported.

64

65 To identify novel host factors that can influence cellular interactions with the SARS-CoV-2 Spike
66 protein, we used a whole genome CRISPR activation approach. Using the Calabrese Human
67 CRISPR Activation Pooled Library[5], we identified a TLR-related cell surface receptor named
68 leucine-rich repeat-containing protein 15 (LRRC15) as a novel SARS-CoV-2 Spike binding
69 protein in three independent whole genome screens, and confirmed this interaction via flow
70 cytometry, immunoprecipitation and confocal microscopy. *LRRC15* is primarily expressed in
71 innate immune barriers including placenta, skin, and lymphatic tissues as well as perturbed-state
72 tissue fibroblasts, and we found LRRC15 protein is absent in control lungs, but highly expressed
73 in COVID-19 patients, where it lines the airways. Mechanistically, LRRC15 is not a SARS-CoV-
74 2 entry receptor, but can antagonise SARS-CoV-2 infection of $ACE2^{+}$ cells when expressed on
75 nearby cells. At the cellular level, LRRC15 is expressed in fibroblasts and these cells increase with
76 COVID-19 infection. Moreover, by RNA seq, we found expression of LRRC15 drives a specific

77 antiviral response in fibroblasts while suppressing collagen gene expression. In summary, we show
78 LRRC15 physically links SARS-CoV-2 to perturbed-state fibroblasts, where LRRC15 expression
79 can control the balance between fibrosis and antiviral responses, and this activity may help
80 promote COVID-19 resolution while preventing COVID-19 lung fibrosis.
81
82 **Results**
83
84 *High throughput SARS-CoV-2 Spike binding assay*
85 Based on *a priori* knowledge of SARS-CoV-1, ACE2 was rapidly identified as the primary
86 receptor for SARS-CoV-2 Spike protein[3]. To investigate other host factors that modulate cellular
87 interactions with SARS-CoV-2 Spike, we employed a pooled CRISPR activation (CRISPRa)
88 screening approach. To this end, we developed a novel cellular flow cytometry-based SARS-CoV-
89 2 Spike binding assay using Alexa Fluor 488-labeled Spike protein (Spike488; **Fig. 1a**). While
90 wild-type HEK293T (WT HEK293T) cells that express low levels of ACE2 show minimal binding
91 to Spike488, when we provided *ACE2* cDNA HEK293T-*ACE2* cells exhibited high Spike488
92 binding activity (**Fig. 1b**). To assess the sensitivity of this assay, we mixed HEK293T-*ACE2* and
93 WT HEK293T cells at various ratios and then measured Spike488 binding by flow cytometry. An
94 increase in Spike488-binding cells could be detected when as little as 1% of the total population
95 was $ACE2^{+}$, indicating that this assay has sufficient sensitivity to enable genome-wide screens
96 (**Fig. 1c**). To perform a pooled CRISPRa screen with this system, we generated a stable HEK293T
97 cell line expressing CRISPRa machinery (*MS2-p65-HSF + VP64*; HEK293T-CRISPRa) (**Fig. 1d**).
98 We tested HEK293T-CRISPRa clones for the ability to induce *ACE2* expression using 3
99 independent single guide RNAs (sgRNAs)[6]. We selected Clone 1 for further use, since it induced

100 similar levels of *ACE2* expression compared to cDNA overexpression, (**Supplementary Fig. 1a**),
101 and confirmed that CRISPRa induction of ACE2 expression conferred Spike488 binding by flow
102 cytometry (**Fig. 1e**).
103
104 *CRISPR activation screening for regulators of SARS-CoV-2 Spike binding identifies LRRC15*
105 Having established the utility of our system, we used the Calabrese Human CRISPR Activation
106 Pooled guide Library[5] to drive CRISPRa-dependent expression of the human genome in
107 HEK293T-CRISPRa cells. Cells were infected with lentivirus-packaged CRISPRa sgRNAs and
108 then selected on puromycin to enrich for transduced cells. Transduced cells were incubated with
109 Spike488 and sorted by FACS to isolate CRISPRa-*sgRNA* cells with enhanced Spike binding.
110 Overall, pooled CRISPRa-*sgRNA* cells showed more Spike binding than mock-transduced controls
111 (**Supplementary Fig. 1b-c**). Genomic DNA (gDNA) was collected from unselected or Spike488-
112 selected cells and sgRNA abundance quantified by sequencing (**Fig. 2a**) and then data analyzed
113 using the MAGeCK analysis platform (v0.5.9.2)[7] and plotted using MAGeCKFlute (v1.12.0)[8].
114 Using an FDR cut off of 0.25, our top hit was the transmembrane protein LRRC15 (LogFC 4.748,
115 P value 2.62×10^{-7}, FDR 0.00495), followed by the SARS-CoV-2 entry receptor ACE2 (LogFC
116 2.1343, P value 2.65×10^{-5}, FDR 0.25). (**Fig. 2b-d; Supplementary Table 1**). Moreover, we
117 conducted 2 additional screens under slightly different conditions, and in all screens our top hit
118 was LRRC15 (**Supplementary Fig. 2a-f**).
119
120 We expressed the *LRRC15* sgRNAs that were hits in our screens in HEK293T-CRISPRa cells and
121 confirmed that they induce expression of *LRRC15* (~approximately 2000-fold induction,
122 **Supplementary Fig. 2g**). Moreover, LRRC15-overexpressing cells dramatically increased SARS-

123 CoV-2 Spike488 binding, with *LRRC15* sgRNA 1 inducing binding to levels comparable to cells
124 overexpressing *ACE2* sgRNA3 (**Fig. 2e**). LRRC15 overexpression did not itself upregulate *ACE2*
125 transcription, suggesting the increased Spike binding in LRRC15-expressing cells is independent
126 of ACE2 upregulation (**Supplementary Fig. 2h**). Conversely, only one of the three *ACE2* sgRNAs
127 from the Calabrese library efficiently activated *ACE2* expression (**Supplementary Fig. 2i-j**),
128 explaining why *ACE2* itself was not a higher ranked hit in our 3 CRISPRa screens (**Fig. 2d,**
129 **Supplementary Fig. 2a-f**). To avoid spectral overlap with GFP-expressing cell lines we
130 conjugated Spike with Alexa Fluor 647 (Spike647), which was used for the rest of the study. Using
131 *ACE2* sgRNA3 and *LRRC15* sgRNA1 cells, we measured 11.6 nM affinity for ACE2/Spike647,
132 which is similar to previous estimates (range: 4.7 - 133.3 nM[9–11]) and 68.8 nM for
133 LRRC15/Spike647 (**Fig. 2f**).
134
135 *LRRC15 is a new transmembrane SARS-CoV-2 Spike receptor*
136 LRRC15 is a 581 amino acid (a.a.) leucine-rich repeat (LRR) protein with 15 extracellular LRRs
137 followed by a single transmembrane domain and a short 22 a.a. intracellular domain (**Fig. 3a and**
138 **3b**). LRRC15 belongs to the LRR Tollkin subfamily that includes TLR1-13 and is most closely
139 related to the platelet von Willebrand factor receptor subunit Glycoprotein V (GP5)[12] (**Fig. 3c**, full
140 tree in **Supplementary Fig. 3a**). To confirm a role for LRRC15 in SARS-CoV-2 Spike binding
141 and ensure the interaction was not an artifact of our CRISPRa strategy, we transfected *LRRC15-*
142 *GFP* cDNA into HEK293T cells and observed Spike647 binding by flow cytometry. There are
143 two reported isoforms of LRRC15 (LRRC15_1 and LRRC15_2), with LRRC15_1 having 6
144 additional amino acids at the N-terminus. Although cells transfected with *GFP* alone showed no
145 binding to Spike647, cells expressing *LRRC15* isoform 1 or 2 both showed strong Spike binding

146 (**Fig. 3d**). While LRRC15-dependent Spike binding was higher than cells stably expressing ACE2
147 (62.1% and 64.5% vs. 48.8%), co-expression of LRRC15 with ACE2 was additive resulting in
148 86.3% positive (LRRC15_1) or 83.8% positive (LRRC15_2) cells (**Fig. 3e**). Interestingly, all cells
149 (100%) stably expressing ACE2 and TMPRSS2 bound Spike647 regardless of LRRC15
150 expression (**Fig. 3f**). However, LRRC15 expression in HEK293T-*ACE2*-*TMPRSS2* cells still
151 enhanced the amount of cell surface Spike647 bound by each cell as measured by mean
152 fluorescence intensity (**Fig. 3g**). Moreover, both *LRRC15* isoforms colocalized with Spike647
153 (**Fig. 3h**). To independently confirm an interaction between LRRC15 and SARS-CoV-2 Spike
154 protein, we added Spike to LRRC15-expressing cells, immunoprecipitated LRRC15, then blotted
155 for both LRRC15 and Spike. While control *GFP*-transfected HEK293T cells did not show any
156 signal at the size predicted for Spike (~200 kDa[13]) (**Supplementary Fig. 3b-c**), when we pulled
157 down either LRRC15_1 or LRRC15_2, in both cases we co-immunoprecipitated Spike protein in
158 the eluate (**Fig. 3i**). Taken together, these data show that LRRC15 expression is sufficient to confer
159 SARS-CoV-2 Spike binding to HEK293T cells, and LRRC15 can further enhance Spike
160 interactions in the presence of ACE2 and TMPRSS2.
161
162 *LRRC15 is not a SARS-CoV-2 entry receptor but can suppress Spike-mediated entry*
163 We next asked if LRRC15 can act as a receptor for SARS-CoV-2 and mediate viral entry. For this
164 we used a SARS-CoV-2 pseudotyped lentivirus system (SARS-CoV-2 pseudovirus) that displays
165 the SARS-CoV-2 Spike protein and carries a luciferase reporter. LRRC15 did not confer SARS-
166 CoV-2 pseudovirus tropism in HEK293T WT (**Supplementary Fig. 4a**) and HEK293T-*ACE2*
167 cells across a wide range of LRRC15 or pseudovirus doses (**Supplementary Fig. 4b**). We then
168 tested if LRRC15 expression impacted infection of HEK293T-*ACE2* and HEK293T-*ACE2*-

169 *TMPRSS2* cells. Indeed, LRRC15-expression in HEK293T-*ACE2* or HEK293T-*ACE2-TMPRSS2*
170 cells show a relatively strong ability to suppress SARS-CoV-2 pseudovirus infection
171 (**Supplementary Fig. 4c-d**). Next we tested if LRRC15 expression can also suppress viral
172 replication and cytopathic effect in infection with authentic SARS-CoV-2 virus. HEK293T-*ACE2-*
173 *TMPRSS2* cells were infected with increasing doses of SARS-CoV-2 (Wuhan variant,
174 **Supplementary Fig. 4e**) and cell death was assessed 48 h later. Ectopic expression of LRRC15
175 did not inhibit infection (two-way ANOVA, $p = 0.378$). Together, these data show that LRRC15
176 is not sufficient to confer SARS-CoV-2 tropism. Instead LRRC15 can limit SARS-CoV-2 spike-
177 mediated entry in *cis*, but once replication competent virions have entered cells, LRRC15 cannot
178 protect infected cells from death.
179
180 *LRRC15 is found on lung fibroblasts that are not infected by SARS-CoV-2*
181 At the tissue level, *LRRC15* RNA is most abundant in the placenta, with expression also found in
182 skin, tongue, tonsils, and lung[14]. At the single cell level, we used the COVID-19 Cell Atlas data
183 set to confirm *LRRC15* expression in placenta decidua stromal cells[15], multiple lymphatic
184 vessels[16–19], and fibroblasts from the skin[20], prostate[21] and lung[17,22–26] (**Fig. 4a**). In the lung[26] (**Fig.**
185 **4b**), we found *LRRC15* is primarily expressed in fibroblasts as well as a population annotated as
186 "neuronal cells" (**Fig. 4c**), and these populations were not infected with SARS-CoV-2 (**Fig. 4d**).
187 These data were corroborated by two other COVID-19 patient single cell/nucleus RNAseq data
188 sets that show similar *LRRC15* fibroblast expression profiles (**Supplementary Fig. 5a-f**), and
189 again LRRC15^{+} cells were not infected with SARS-CoV-2[24] (**Supplementary Fig. 5c**). Of note,
190 the viral RNA detected was low in these patients. Together, these data support our *in vitro*
191 observations that LRRC15 does not mediate SARS-CoV-2 infection but may instead act as an

192 innate immune barrier. In contrast, ACE2 was detected primarily in uninfected type I (AT1) and
193 (AT2) alveolar epithelium (**Fig. 4d)**, and SARS-CoV-2-infected alveolar epithelium ("Other
194 epithelial cells") that lost AT1/2 markers and upregulated ribosomal transcripts consistent with
195 viral infection and cell death. We next assessed LRRC15 protein expression in human lung
196 parenchyma. We observed that COVID lungs have epithelial metaplasia, more immune infiltrate
197 and intra alveolar fibroblast proliferation (**Fig. 4e-f, Supplementary Fig. 6a**). This matches with
198 single cell RNA seq that shows lung fibroblasts increases significantly during COVID-19 (7.9%
199 in control and 22.9% in COVID-19 patients; **Fig. 4g**). Moreover, we found that LRRC15 is present
200 on the alveolar surface of lung tissue samples from donors with COVID-19, but not present in
201 control lungs from individuals without COVID-19, and LRRC15 expression was mutually
202 exclusive with collagen (**Fig. 4h-i, Supplementary Fig. 6b)**.
203
204 While HEK293T cells do not express *LRRC15*, the human fibroblast line IMR90 does (**Fig. 5a**).
205 In the rat glia cell line C6 *LRRC15* is mildly regulated in response to proinflammatory cytokines
206 like IL1β, IL6, and TNFα[27], and more recently TGFβ signalling has been linked to LRRC15
207 expression in cancer-associated fibroblasts[28,29]. In human fibroblasts, we found IL1β, TNFα or
208 IFNɣ do not induce detectable levels of LRRC15 (not shown), however TGFβ upregulates both
209 *LRRC15* (**Fig. 5b**) and *COL1A1* transcripts (**Fig. 5c**) and LRRC15^{+} fibroblasts bind SARS-CoV-
210 2 Spike protein (**Supplementary Fig. 7a**). Moreover, ectopic expression of LRRC15 is also
211 sufficient to enhance SARS-CoV-2 Spike binding on fibroblasts (**Fig. 5d**), however LRRC15
212 expression was again not sufficient to confer SARS-CoV-2 pseudovirus tropism (**Fig. 5e)**. Since
213 human lung fibroblasts express LRRC15 and are not infected with SARS-CoV-2, we reasoned that
214 LRRC15 may act to bind and sequester SARS-CoV-2 virions away from ACE2^{+} target lung

215 epithelium. In human COVID-19 patients, fibroblasts and epithelial cells are present at a ratio of
216 ~2:1 (**Fig. 5f**). Thus to test if LRRC15 can sequester virus and suppress SARS-CoV-2 infection,
217 we co-cultured fibroblasts expressing *LRRC15-GFP* with SARS-CoV-2 permissive HEK293T-
218 *ACE2-TMPRSS2* at a ratio of 2:1. Indeed we found LRRC15^{+} fibroblasts can antagonise infection
219 of both SARS-CoV-2 pseudovirus (**Fig. 5g**) and authentic SARS-CoV-2 virus (Wuhan, **Fig. 5h**).
220 Thus, together we show LRRC15 is expressed specifically by lung fibroblasts, is found coating
221 the airways in COVID-19 patients, and mechanistically, LRRC15 can act to sequester SASR-CoV-
222 2 virus and help suppress infection, which may potentially help protect ACE2^{+} alveolar epithelium
223 in patients with COVID-19.
224
225 *LRRC15 is a potent regulator of antiviral and fibrotic programs*
226
227 While we believe the most direct mechanism by which LRRC15 may participate in COVID-19
228 infection is through binding to and sequestering SARS-CoV-2 virions, little is known about the
229 broader role for LRRC15 in physiology or how LRRC15 expression impacts fibroblast
230 transcriptional programs. A recent study on the organization of tissue fibroblasts identified
231 *LRRC15* as a lineage marker for perturbed state activated myofibroblasts[23]. These specialized
232 fibroblasts arise during disease, express collagen and other ECM-modifying genes, and participate
233 in tissue repair and fibrosis[23]. We also observed lung *LRRC15*$^{+}$ myofibroblasts in multiple
234 COVID-19 patient data sets, and these cells also express collagen **(Fig. 6a**). To directly investigate
235 the relationship between LRRC15 and collagen, we generated an LRRC15 overexpressing stable
236 human fibroblast line, then evaluated LRRC15-induced transcriptional changes by RNA seq.
237 Surprisingly, we found driving expression of LRRC15 in fibroblasts induced upregulation of

238 cellular antiviral programs and downregulated expression of collagen transcripts (**Fig. 6b,**
239 **Supplementary Table 5**). These results are clearly visible in the volcano plot (red transcripts were
240 upregulated, blue transcripts down regulated), however they were also captured in pathway
241 analysis (**Fig. 6c, Supplementary Table 6**), where we found interferon and influenza signalling
242 were the most upregulated pathways, whereas wound healing and pulmonary fibrosis were the
243 most downregulated pathways. Of note, pancreatic adenocarcinoma signalling was also highly
244 upregulated, and this is in line with a recent study highlighting the role of LRRC15^{+} fibroblasts in
245 driving disease severity in pancreatic cancer[29] . The primary antiviral pathways upregulated by
246 LRRC15 expression were IFITs (Interferon Induced proteins with Tetratricopeptide repeats), MXs
247 (Myxovirus resistance genes), and OASs (2-prime, 5-prime oligoadenylate synthetases) and we
248 confirmed these data by RT-qPCR (**Fig. 6d**). Moreover, LRRC15 expression had an unexpected
249 and potent ability to downregulate collagen transcripts, and we confirmed this both by RT-qPCR
250 (**Fig. 6e)** and western blotting (**Fig. 6f, Supplementary Fig. 6b).**
251
252 Overall, we describe the TLR-related receptor LRRC15 as a new spike receptor that can bind and
253 sequester SARS-CoV-2 and limit infection. LRRC15 is induced extensively during COVID-19,
254 where it lines the airways and may form an innate antiviral barrier. Surprisingly, while LRRC15
255 is induced on fibroblasts during disease, ectopic expression of LRRC15 switches fibroblast
256 transcriptional programs from a fibrotic program to an antiviral one, and this may help the lung
257 orchestrate innate immunity programs vs. immune resolution and lung repair.
258
259 **Discussion**
260

261 Using an unbiased functional genomics approach, we have identified the leucine rich repeat
262 receptor LRRC15 as a new SARS-CoV-2 inhibitory receptor that can regulate innate immunity
263 and lung repair. LRRC15 promotes SARS-CoV-2 spike binding comparable to ACE2, however
264 LRRC15 is not sufficient to confer viral tropism. LRRC15 is normally highly expressed in tissues
265 that form important immune barriers like the placenta, skin, and various lymphatics, and is related
266 to TLR innate immune receptors[14]. In previous work, LRRC15 has been shown to suppress
267 adenovirus infection[30], and here we show LRRC15 can also bind to and suppress SARS-CoV-2
268 Spike pseudovirus and live SARS-CoV-2 infection. Moreover, in human SARS-CoV-2-infected
269 airways, we see that LRRC15 forms a pronounced barrier-like structure, and given the expression
270 pattern and function of LRRC15, we hypothesize that this molecule is a pattern recognition
271 receptor and innate immune barrier that may play an important role in host defense. Moreover,
272 LRRC15 is found on collagen-producing myofibroblasts and we show ectopic expression of
273 LRRC15 suppresses collagen production and drives antiviral programs, and in this way directly
274 links SARS-CoV-2 with innate antiviral immunity and lung fibrosis.
275
276 Although our data shows that LRRC15 promotes cellular binding to SARS-CoV-2 Spike protein,
277 we also show that LRRC15 does not act as an entry receptor, but instead can inhibit SARS-CoV-
278 2 in *trans*. This observation is consistent with a previous report that LRRC15 can also impede
279 adenovirus infection[30]. We hypothesize that LRRC15 may play a role in limiting SARS-CoV-2
280 transmission by sequestering free virus in the airways of COVID-19 patients, and the LRRC15 we
281 observed lining the airways may also suppress collagen deposition protecting the airways from
282 fibrosis during some stages of lung infection. It is likely that the role for LRRC15 in lung immunity
283 is more broad than just interactions with SARS-CoV-2, and LRRC15 may represent a new

284 fibroblast-expressed pattern recognition receptor that can bind to and sequester a variety of
285 microbial antigens, however this remains to be established.
286
287 LRRC15 is a member of the LRR superfamily and LRR-Tollkin subfamily of LRR-containing
288 proteins, many of which play critical roles in host defense[12]. Of the TLR family, LRRC15 is most
289 related to TLR5, which also recognises a major extracellular virulence factor, the bacterial
290 extracellular protein flagellin[31]. Remarkably, while our manuscript was in preparation and then
291 review, two other groups independently released preprints describing similar ORF/CRISPR
292 activation screening strategies to identify new host factors that can regulate Spike binding; both
293 screens also pulled out LRRC15 as a top factor driving Spike/host cell interactions[32,33]. These
294 studies corroborate our findings, despite their use of different Spike formulations, overexpression
295 strategies, and cell lines. Moreover, since our initial submission[34], Song et al. have replicated our
296 finding that LRRC15 can act in *trans* to suppress SARS-CoV-2 infections and this has now been
297 published[33]. Together, our studies highlight a fundamental new role for LRRC15 in SARS-CoV-2
298 biology and likely beyond.
299
300 Several CRISPR Loss of Function (LOF) and Gain of Function (GOF) screens have been reported
301 in attempts to identify novel SARS-CoV-2 interactors and regulators. Though these CRISPR
302 screens have been successful in identifying novel SARS-CoV-2 receptors and co-receptors[35–39],
303 ACE2-regulators[40,41], complexes such as the vacuolar ATPase proton pump, Retromer,
304 Commander and SWI/SNF chromatin remodeling machinery[40,41] and have implicated many new
305 pathways in SARS-CoV-2 infection[36,38,41], they have all failed to identify LRRC15. This difference
306 is likely due to screening with SARS-CoV-2 authentic virus and pseudovirus screens being unable

307 to divorce Spike binding from downstream effects of infection. Our fluorophore-conjugated Spike
308 protein/pooled CRISPR screening model thus represents a new and complementary paradigm for
309 investigating host/virus interactions or virtually any other cell surface interaction.
310
311 Our data suggests the primary mechanism of action for LRRC15 in the context of SARS-CoV-2
312 infection is likely through a direct interaction with the Spike protein that sequesters SARS-CoV-2
313 virions and in this way helps to limit infection. Beyond this, we show that LRRC15 also has a
314 potent and specific impact on fibroblast gene expression, suppressing collagen while enhancing
315 antiviral programs. We found LRRC15 expression caused an upregulation of 3 antiviral pathways,
316 IFIT, MX, and OAS, and these antiviral pathways are also upregulated in primates infected with
317 SARS-CoV-2[42] and COVID-19 patients[43]. IFIT proteins are induced by IFN, viral infection, or
318 PAMP recognition, where they can then directly bind to viral RNA, block viral translation, and
319 activate cellular antiviral responses[44]. A recent preprint found the SARS-CoV-2 nonstructural
320 protein NSP16 helps SARS-CoV-2 evade the host antiviral immune response by avoiding the
321 antiviral activities of IFIT1 and 3[45]. MX proteins are interferon-induced dynamin-like GTPases
322 with antiviral activity against multiple RNA and DNA viruses. For example MX1 can block
323 influenza A by altering sorting of viral vesicles in the ER / Golgi intermediate compartment[46]. In
324 COVID-19, MX1 is upregulated with increasing viral load[47], and functionally, the SARS-CoV-2
325 protein ORF6 can suppress MX1 induction[48]. OAS proteins are dsRNA sensors that can activate
326 RNAse L which then degrades viral RNA and inhibits protein synthesis[49]. Importantly, OAS1 is a
327 potent host antiviral factor that can block SARS-CoV-2 infection *in vitro*, and OAS1 expression
328 also associates with protection from severe COVID-19 outcome *in vivo*[50].
329

330 While our data highlights a new role for LRRC15 in promoting SARS-CoV-2 Spike binding,
331 limiting infection, and regulating collagen expression, it is currently unclear how LRRC15
332 contributes to human COVID-19 disease. Notably, while this manuscript was under revision, a
333 preprint authored by Gisby et al. investigated serum from control and COVID-19 infected end
334 stage kidney disease patients, and found that out of the entire serum proteome, depletion of
335 circulating LRRC15 is the strongest predictor of COVID-19 clinical outcome[51]. Integrating these
336 data, it is possible that fibroblast-expressed LRRC15, or potentially cell free LRRC15 deposits in
337 the airways, could trap viral particles for subsequent clearance by the innate immune system, while
338 at the same time enhancing cellular antiviral tone and suppressing fibrosis. LRRC15 may even
339 help fibroblasts pass immobilized virus to innate lung antigen presenting cells, as a recent spatial
340 transcriptomics study showed that lung fibroblasts interact with both SARS-CoV-2 Spike^{+}
341 macrophages and dendritic cells[52]. If lung LRRC15/SARS-CoV-2 complexes are depleted, and
342 new LRRC15 is not produced, this may lead to a detectable decrease in serum LRRC15 that is
343 indicative of poor COVID-19 outcome. While it is clear that LRRC15 is an important new
344 component of our innate immune system, the precise mechanisms of action of LRRC15 during
345 COVID-19 infection remain to be established.
346
347 Overall, our unbiased functional genomic investigation of SARS-CoV-2 Spike/host interactions
348 identified the novel TLR-related receptor LRRC15 as a powerful host factor driving SARS-CoV-
349 2 Spike interactions and controlling both antiviral and anti-fibrotic responses. Further investigation
350 into how LRRC15 contributes to innate immunity can help us better understand and treat this and
351 future pandemics.
352

353 **Lead contact**

354 Further information and requests for resources and reagents should be directed to and will be
355 fulfilled by the lead contact, Graham G. Neely (greg.neely@sydney.edu.au).

356

357 **Materials availability**

358 This study did not generate any new unique reagents.

359

360 **Data and code availability**

361 CRISPR screen raw read counts have been deposited at GSE186475 and are publicly available as
362 of the date of publication. CRISPR screen analysis is shown in **Fig. 2** and **Supplementary Fig. 2.**
363 CRISPR screen output is reported in **Supplementary Table 1**. RNA sequencing bam files have
364 been deposited on NCBI SRA at PRJNA895078 and are publicly available as of the date of
365 publication. Analysis of RNA sequencing data is shown in **Fig. 6**. Results of differential gene
366 expression analysis are reported in **Supplementary Table 5**. Canonical Pathways output from
367 Ingenuity Pathway Analysis is reported in **Supplementary Table 6**. This paper also analyzes
368 existing publicly available single cell RNA-sequencing data (GSE158127, SCP1052, SCP1219).
369 All data reported in this paper will be shared by the lead contact upon request. This paper does not
370 report original code. Any additional information required to reanalyze the data reported in this
371 paper is available from the lead contact upon request.

372

373 **Experimental model and subject details**

374

375 **Cell culture**

376 HEK293T cells (female; ATCC, CRL-3216, RRID: CVCL_0063) were cultured in Dulbecco's
377 Modified Eagle Medium (ThermoFisher Scientific, Cat #11995065) with 10% HyClone Fetal
378 Bovine Serum (Cytiva, SH30084.03) and 1% Penicillin-Streptomycin (Gibco, 15140122) at 37°C,
379 5% CO_2 and atmospheric oxygen. IMR90 *E6E7* (female) human fibroblast cells were a gift from
380 Anthony Cesare (Children's Medical Research Institute, Sydney, Australia). IMR90 were cultured
381 in DMEM (ThermoFisher Scientific, 11995065) supplemented with 10% HyClone FBS (Cytiva,
382 SH30084.03) and 1x non-essential amino acids (Gibco, 11140050) at 37°C, 3% O_2 and 10% CO_2.
383 Expi293F™ cells (female; ThermoFisher Scientific, A14527, RRID:CVCL_D615) were cultured
384 in Expi293™ Expression Medium (ThermoFisher Scientific, A1435101) with 5% CO_2 and
385 atmospheric O_2 at 37 °C for 24 h and then lowered to 32 °C for 72 h. Cell lines have been
386 authenticated.
387
388 **Method Details**
389
390 **Generation of CRISPR activation cell line**
391 HEK293T cells were co-transfected with pPB-
392 R1R2_EF1aVP64dCas9VP64_T2A_MS2p65HSF1-IRESbsdpA (Addgene #113341) and the
393 Super PiggyBac Transposase Expression Vector (System Biosciences, PB210PA-1) using
394 Lipofectamine 3000 Transfection Reagent (ThermoFisher Scientific). These cells (HEK293T-
395 CRISPRa) were then selected on blasticidin (Merck) at 5 µg/mL for 10 days prior to clonal
396 isolation and expansion. These cells express synergistic activation machinery (SAM), which
397 includes VP64-dCas9-VP64 fusion protein and helper proteins MS2, p65 and HSF. When

398 transduced with pXPR_502 (Addgene #96923) single guide RNA (sgRNA) plasmid, the cells also
399 express PCP-p65-HSF complex which is recruited to PP7 aptamers in the sgRNA scaffold [5].
400
401 **sgRNA vector cloning**
402 Single guide RNA (sgRNA) sequences for non-targeting control and ACE2 were taken from the
403 Weissman Human Genome-wide CRISPRa-v2 library (Addgene #83978). LRRC15 sgRNA
404 sequences and additional ACE2 sgRNA sequences were taken from the Human CRISPR activation
405 pooled library set A (Addgene #92379). Sense and antisense strands for each sequence were
406 ordered as DNA oligonucleotides (IDT) with 5' overhangs of 5'-CACC-3' on the sense strand
407 oligonucleotide and 5'-AAAC-3' on the antisense strand oligonucleotide. Oligonucleotides were
408 annealed at 4°C for 16 h and pXPR-502 (Addgene #96923) was digested with Esp3I
409 (ThermoFisher Scientific, ER0451) or BsmBI-v2 (New England Biolabs). sgRNA DNA
410 oligonucleotide duplexes were ligated into the digested pXPR-502 backbone using T4 ligase (New
411 England Biolabs) and incubated at 4°C overnight. NEB 10-beta competent *E. coli* (New England
412 Biolabs) were transformed with 100 ng of each sgRNA construct by heat-shock, plated onto LB-
413 agar plates (Life Technologies) containing ampicillin (Sigma-Aldrich) and grown at 37°C.
414 Individual colonies were picked, expanded in Luria broth (Life Technologies) supplemented with
415 ampicillin and amplified constructs were harvested using either ISOLATE II Plasmid Mini Kit
416 (Bioline) or PureYield Plasmid Maxiprep System (Promega Corporation).
417
418 **Whole genome sgRNA library amplification**
419 MegaX DH10B T1^{R} Electrocomp™ Cells (ThermoFisher Scientific) were electroporated with 400
420 ng Human CRISPR activation pooled library set A (Addgene #92379) and left to recover in

421 Recovery Medium for 1 hour at 37°C. Cells were then spread on 600 cm^2 LB-agar plates
422 supplemented with carbenicillin (Merck) and incubated at 37°C for 16 hours. All colonies were
423 scraped, collected and processed using the PureYield Plasmid Maxiprep System (Promega
424 Corporation). The concentration of the plasmid library was determined via Nanodrop
425 (ThermoFisher Scientific).
426
427 **Lentivirus production and viral transduction**
428 Lipofectamine 3000 Transfection Reagent (ThermoFisher Scientific) in Opti-MEM Medium
429 (Gibco) was used to co-transfect HEK293T cells with psPAX2 (Addgene #12260), pCAG-VSVg
430 (Addgene #35616) and either individual sgRNA constructs ligated into pXPR-502 (Addgene
431 #96923) or pooled CRISPRa library (Human CRISPR activation pooled library set A, Addgene
432 #92379) according to the manufacturer's instructions. Cells were incubated with transfection
433 reagents for 16 h before the media was replaced. Viral media was collected 24 h later. For
434 individual sgRNA constructs, neat viral media was added to HEK293T-CRISPRa cells with
435 Polybrene Infection / Transfection Reagent (Sigma-Aldrich) at a concentration of 8 µg/mL. Viral
436 media was replaced with fresh medium the following day and puromycin dihydrochloride (Gibco)
437 added 24 h later at a concentration of 1.6 µg/mL for 72 h selection. For sgRNA library virus, viral
438 media was passed through a 0.45 µm filter (Merck Millipore) and concentrated using 100K
439 MWCO Pierce Protein Concentrators (Life Technologies Australia). Concentrated virus was then
440 stored at -80°C.
441
442 **SARS-CoV-2 Spike protein production**

443 The expression construct for recombinant soluble trimeric SARS-CoV-2 spike protein (residues
444 1-1208, complete ectodomain) was generously provided by Dr Florian Krammer (Icahn School of
445 Medicine, Mt Sinai). This protein was used for the initial setup of the screen (shown in Fig. 1) and
446 in one CRISPRa screen (Screen 2). This construct includes the SARS-CoV-2 Spike native signal
447 peptide (residues 1-14) to target the recombinant protein for secretion, stabilising proline
448 substitutions at residues 986 and 987, substitution of the furin cleavage site (residues 682-685)
449 with an inert GSAS sequence, and a C-terminal His6-tag to enable affinity purification.
450
451 Soluble trimeric SARS-CoV-2 spike was expressed in EXPI293F™ cells via transient transfection
452 using 25 kDa linear polyethyleneimine (PEI) (Polysciences Inc.). EXPI293F™ cultures were
453 grown at 37°C, with shaking at 130 rpm, to a cell density of $3x10^6$ cells/mL before transfection
454 with pre-formed SARS-CoV-2 spike plasmid DNA:PEI complexes (2 µg/mL DNA and 8 µg/mL
455 PEI). The transfected cells were incubated at 37°C for 24 h and then at 32°C for a further 72 h
456 before harvesting. Culture medium, containing secreted SARS-CoV-2 spike, was harvested by
457 centrifugation at 4000 xg for 20 min. Supernatants from the centrifugation step were supplemented
458 with 20 mM HEPES (pH 8.0) and subjected to immobilised metal affinity chromatography
459 (IMAC) by incubation with Ni-NTA agarose pre-equilibrated with a buffer consisting of 20 mM
460 NaH_2PO_4 (pH 8.0), 500 mM NaCl, and 20 mM imidazole. His6-tagged SARS-CoV-2 spike protein
461 was eluted from the Ni-NTA agarose using a buffer comprising 20 mM NaH_2PO_4 (pH 7.4), 300
462 mM NaCl, and 500 mM imidazole. Eluates from affinity chromatography were concentrated and
463 further purified by gel filtration chromatography using a Superdex 200 10/30 GL column (Cytiva)
464 and buffer consisting of 20 mM HEPES (pH 7.5) and 150 mM NaCl. The quality of protein
465 purification was assessed by SDS-PAGE and multiple angle laser light scattering (MALLS).

466

467 The expression construct for a more stable variant of soluble trimeric SARS-CoV-2 spike
468 ectodomain protein called "HexaPro" was a gift from Jason McLellan (Addgene, #154754). This
469 "Hexapro" protein was used in 2 CRISPRa screens (Screen 1 and 3) and in all validation
470 experiments. This construct, in addition to above, includes 6 total stabilising proline substitutions
471 at residues 817, 892, 899, 942, 986 and 987. The protein was expressed, and the culture medium
472 was harvested as above. The supernatant containing the protein was supplemented with 20 mM
473 HEPES pH 8.0 and subjected to IMAC with Ni-NTA as above. The eluate was dialysed to a buffer
474 containing 2 mM Tris (pH 8.0) and 200 mM NaCl and concentrated to reduce the total volume by
475 a factor of 3. The sample was passed through a 0.22 µm filter and purified by gel filtration
476 chromatography using HiLoad 16/600 Superdex 200 (Cytiva) in a buffer composed of 2 mM Tris
477 (pH 8.0) and 200 mM NaCl. The quality of the protein was assessed by SDS-PAGE and MALLS.

478

479 **Conjugation of SARS-CoV-2 Spike glycoprotein with fluorophores**

480 Spike protein was conjugated to Alexa Fluor™ 488 or Alexa Fluor™ 647 using protein labelling
481 kits (Invitrogen) according to manufacturer's instructions. Briefly, 50 µL of 1 M sodium
482 bicarbonate was added to 500 µl of 2 mg/mL Spike protein. The solution was then added to room
483 temperature Alexa Fluor™ 488 or 647 reactive dye and stirred for 1 h at room temperature.
484 Conjugated Spike proteins were loaded onto Bio-Rad BioGel P-30 Fine size exclusion purification
485 resin column and eluted via gravity (Alexa Fluor™ 488) or centrifugation (Alexa Fluor™ 647).
486 NanoDrop (ThermoFisher Scientific) was used to determine protein concentration.

487

488 **Generation of ACE2 and dual ACE2/TMPRSS2 cDNA overexpression cell lines**

489 HEK293T cells stably expressing human ACE2 (HEK293T-*ACE2*) were generated by transducing
490 HEK293T cells with a lentivirus expressing *ACE2*[53]. Briefly, ACE2 ORF was cloned into a 3rd
491 generation lentiviral expression vector, pRRLsinPPT.CMV.GFP.WPRE[54] using Age1/BsrG1 cut
492 sites, thus replacing *GFP ORF* with *ACE2* to create a novel expression plasmid, herein referred to
493 as ppt-*ACE2*. Lentiviral particles expressing ACE2 were produced by co-transfecting ppt-*ACE2*,
494 a 2nd generation lentiviral packaging construct psPAX2 and VSV-G plasmid pMD2.G (Addgene
495 #12259) in HEK293T cells by using polyethylenimine as previously described[55]. Virus supernatant
496 was harvested 72 hours post transfection, pre-cleared of cellular debris and centrifuged at 28,000
497 xg for 90 minutes at 4 °C to generate concentrated virus stocks. To transduce HEK293T cells,
498 10,000 cells per well were seeded in a 96 well tissue culture plate and virus supernatant added in
499 a 2-fold dilution series. At 72 hours post transduction the surface expression of ACE2 was
500 measured by immunostaining the cells with anti-ACE2 monoclonal antibody (Thermo Fisher
501 Scientific, MA5-32307). Cells showing maximal expression of ACE2 were then sorted into single
502 cells using BD FACS Aria III cell sorter to generate clonal populations of HEK293T-*ACE2* cells.
503
504 For generating HEK293T cells expressing both ACE2 and TMPRSS2 (HEK293T-*ACE2*-
505 *TMPRSS2*), HEK293T-*ACE2* cells described above were transduced with lentiviral particles
506 expressing *TMPRSS2*. To achieve this, *hTMPRSS2a* (synthetic gene fragment; IDT) was cloned
507 into lentiviral expression vector pLVX-IRES-ZsGreen (Clontech) using EcoR1/XhoI restriction
508 sites and lentiviral particles expressing *TMPRSS2* were produced as described above. Lentiviral
509 transductions were then performed on HEK293T-*ACE2* cells to generate HEK293T-*ACE2*-
510 *TMPRSS2* cells. Clonal selection led to the identification of a highly permissive clone, HekAT24[53],
511 which was then used in subsequent experiments.

512

513 **Optimizing a flow cytometry-based assay for determining SARS-CoV-2 Spike binding**

514 HEK293T-*ACE2* cells were dissociated by incubating with TrypLE for 5 min at 37°C and
515 neutralized with DMEM. 10^6 cells were collected, washed with 1% bovine serum albumin (BSA;
516 Sigma-Aldrich) in Dulbecco's Phosphate Buffered Saline (DPBS; Sigma-Aldrich) and then
517 incubated with increasing concentrations of Alexa Fluor 488-conjugated SARS-CoV-2 spike
518 glycoprotein (Spike488) for 30 min at 4°C. The cells were then washed once with DPBS before
519 resuspending in 1% BSA in DPBS and analyzed using the Cytek Aurora (Cytek Biosciences). For
520 cell mixing experiments, increasing proportions of HEK293T-*ACE2* cells (0%, 1%, 20%, 50%,
521 80% and 100%) were combined with decreasing proportions of wildtype (WT) HEK293T cells
522 (100%, 99%, 80%, 50%, 20%, 0%) to a total of 10^6 cells per sample. These samples were incubated
523 with 50 μg/mL Spike488 as described above and analyzed using the Cytek Aurora (Cytek
524 Biosciences).

525 To confirm the validity of this assay in detecting binding in cells expressing CRISPRa machinery,
526 a clonal line of HEK293T with stable expression of a plasmid encoding dCas9-VP64 and SAM
527 system helper proteins (pPB-R1R2_EF1aVP64dCas9VP64_T2A_MS2p65HSF1-IRESbsdpA)
528 (HEK293T-CRISPRa) was transduced with lentivirus carrying *ACE2* sgRNA 1 or non-targeting
529 control sgRNA. These cells were then incubated with Spike488 as previously described and
530 analyzed on the Cytek Aurora (Cytek Biosciences).

531

532 **CRISPR activation screening**

533 HEK293T-CRISPRa cells were transduced with concentrated Human CRISPR activation pooled
534 library set A (Addgene #92379)-carrying lentivirus at a multiplicity of infection (MOI) of

535 approximately 0.3. Cells were selected on puromycin dihydrochloride (Gibco) at a concentration
536 of 1.6 μg/mL for 3 days (screen 1 and 2). $3x10^7$ cells (>500 cells/guide) were incubated with
537 Spike488 for 30 min at 4°C, washed to remove excess spike protein, and sorted for increased Alexa
538 Fluor 488 intensity using the BD FACSMelody Cell Sorter (BD Biosciences). Gates for flow
539 assisted cytometric sorting were set using non-targeting control (NTC) sgRNA-transduced cells as
540 a negative control and *ACE2* sgRNA-transduced cells as a positive control, both of which had been
541 incubated with Spike488 under the same conditions as stated previously. Unsorted cells were
542 maintained separately so as to be used as a diversity control. Cells were expanded and $1.5\text{-}2x10^6$
543 cells were then collected for genomic DNA (gDNA) extraction for sorted samples and $3x10^7$ for
544 the unsorted diversity control. Remaining diversity control cells were re-seeded and once again
545 incubated with Spike488 under the same conditions as stated previously (screen 3). These Spike-
546 incubated cells were sorted again but selected on puromycin for eight days prior to expansion and
547 collection of $1x10^7$ cells from both the sorted cell population and the unsorted diversity control
548 population for gDNA extraction. Gating strategy is shown in **Supplementary Fig. 1b**.
549
550 gDNA was extracted from all collected cells using the ISOLATE II Genomic DNA Kit (Bioline).
551 Samples were prepared for NGS via PCR. Genomic DNA (25 μg for unsorted diversity control
552 samples, 5 μg for sorted samples) was added to NEBNext High-Fidelity 2X PCR Master Mix (New
553 England Biolabs) and 0.4 μM P5 staggered primer mix and 0.4 μM of P7 indexing primer unique
554 to each sample. PCR cycling conditions and primers were adapted from Sanson et al.[5]. Primer
555 sequences can be found in **Supplementary Table 3**. Briefly, reactions were held at 95°C for 1
556 min, followed by 28 cycles of 94°C for 30 s, 53°C for 30 s and 72°C for 30 s, followed by a final
557 72°C extension step for 10 min. Amplicons were gel extracted and purified using the ISOLATE II

558 PCR & Gel Kit (Bioline) and the quality and concentration of DNA assessed with the High
559 Sensitivity DNA kit (Agilent Technologies). Samples were then sent to Novogene for next
560 generation sequencing. Raw next generation sequencing reads were then processed using
561 MAGeCK (v0.5.9.2)[7] to identify enriched genes. Median normalization was used with gene test
562 FDR threshold set to 0.1. Plots were generated using MAGeCKFlute (v1.12.0)[8] Normalized read
563 counts were produced using MAGeCK 'count' function on each pairing of unsorted diversity
564 control and sorted sample. Mean and standard deviation was calculated for each individual sample
565 (i.e. separately for diversity control and sorted sample) and the Z-score calculated using $Z = \frac{x-\mu}{\sigma}$,
566 where x is the normalized read count for an individual sgRNA, μ is the mean of all normalized
567 read counts in the sample and σ is the standard deviation of all normalized read counts in the
568 sample.
569
570 **Validation of ACE2 and LRRC15 by CRISPRa**
571 To validate the function of LRRC15 in binding SARS-CoV-2 spike, clonal HEK293T-CRISPRa
572 cells were transduced with lentivirus carrying *ACE2* sgRNAs, *LRRC15* sgRNAs or a NTC sgRNA.
573 Cells were selected on 1.6 µg/mL puromycin dihydrochloride (Gibco) for 3 days and then collected
574 for analysis by RT-qPCR and flow cytometry. For validation by flow cytometry, $1x10^6$ cells were
575 incubated with 50 μg/mL Spike647 as previously described and then analyzed using the Cytek
576 Aurora (Cytek Biosciences). Binding affinity of ACE2 and LRRC15 were conducted with *ACE2*
577 sgRNA3 and *LRRC15* sgRNA1 cells with 1, 5, 10, 25, 50 and 100 μg/mL Spike647 (corresponding
578 to 7, 35, 70, 175, 350 and 700 nM) .
579
580 **RNA extraction and RT-qPCR**

581 RNA was isolated from cells using the ISOLATE II RNA Mini Kit (Bioline) and concentration
582 was measured by Nanodrop (Thermo Scientific). cDNA was synthesized using the iScript Select
583 cDNA Synthesis Kit (Bio-Rad) according to manufacturer's instructions. Briefly, 50-500 ng of
584 RNA was added to iScript RT Supermix and nuclease-free water to a final volume of 10 µL. The
585 assembled reactions were then incubated in a thermocycler as follows: 25°C for 5 min, 46°C for
586 20 min and then 95°C for 1 min. RT-qPCR was then performed on the cDNA samples using SYBR
587 Select Master Mix (ThermoFisher Scientific) and the LightCycler 480 System (Roche). All primer
588 sequences used are listed in **Supplementary Table 4**. Results were analyzed using the $\Delta\Delta C_T$
589 method.
590
591 **LRRC15 crystal structure prediction**
592 The predicted crystal structure for LRRC15 was calculated using AlphaFold (v2.0)[56]
593 (https://alphafold.ebi.ac.uk/entry/Q8TF66) and sourced via UniProt[57]
594 (https://www.uniprot.org/uniprot/Q8TF66).
595
596 **LRR Tollkin Phylogenetic Tree**
597 Protein sequences of LRR Tollkin family members[12] were clustered using Clustal Omega
598 (v1.2.2)[58]. The phylogenetic (Newick) tree was visualized with MEGA11[58,59].
599
600 **Validation of LRRC15 independent of CRISPR activation**
601 *LRRC15-TurboGFP* fusion constructs (Origene, RG225990 and RG221437) were used for flow
602 cytometry, immunoprecipitation and immunocytochemistry experiments while *LRRC15-myc-*
603 *DDK* fusion constructs (Origene, RC225990 and RC221437) were utilized for SARS-CoV-2

604 authentic virus inhibition experiments. Both *TurboGFP*-tagged and *Myc-DDK*-tagged *LRRC15*
605 constructs were used in pseudovirus infection experiments assessing *cis*-inhibition of infection.
606 *LRRC15* transcripts were excised from the *LRRC15-TurboGFP* and *LRRC15-myc-DDK* constructs
607 and replaced with multiple cloning sites to generate empty vector controls for transfection.
608
609 To evaluate the role of LRRC15 in binding SARS-CoV-2 spike glycoprotein independent of
610 CRISPR activation machinery, 2.5 µg of plasmids carrying the *GFP*-tagged *LRRC15* cDNA
611 transcript 1 or 2, or empty vector control (pLJM1-EGFP; Addgene #19319) were transfected into
612 HEK293T, HEK293T-*ACE2* and HEK293T-*ACE2-TMPRSS2* cells as described above. For each
613 sample, 10^6 cells were collected and incubated with Alexa Fluor 647-conjugated SARS-CoV-2
614 spike glycoprotein (Spike647) and analyzed using the Cytek Aurora (Cytek Biosciences) as
615 described above.
616
617 **Immunoprecipitation**
618 For SARS-CoV-2 spike pulldown, $2x10^7$ HEK293T cells transfected with *LRRC15-TurboGFP*
619 (transcript 1 and 2) or *pLJM1-EGFP* (Addgene #19319) were incubated with 50 µg/mL spike
620 hexapro for 30 min at 4°C with rotation. Cells were washed with DPBS (Sigma-Aldrich, D8537)
621 and incubated for 15 min in lysis buffer (1% Igepal-CA-630, 5 mM Tris HCl (pH 7.4), 150 mM
622 NaCl, 1 mM $MgCl_2$, 5% glycerol, 10 mM NaF, 10 mM sodium pyrophosphate, 10 mM sodium
623 orthovanadate, 60 mM β-Glycerophosphate, 1X complete EDTA-free protease inhibitor (Roche))
624 on ice. Samples were then sonicated at 90% amplitude for 30 seconds using the BANDELIN
625 SONOPULS mini20 and spun down at 18,000 g for 10 mins. Concentration of protein samples
626 was determined using BCA assay (ThermoFisher Scientific). 1 µg of anti-LRRC15 antibody

627 (Abcam, EPR8188(2)) or rabbit IgG (Covance, CTL-4112) was added to 1 mg protein lysate and
628 incubated at 4°C with rotation for 2.5 h before precipitation with protein G (ThermoFisher
629 Scientific). Immunoprecipitated proteins were eluted with 0.1 M Tris and 4% SDC. Input, flow-
630 through and eluate were mixed with 4X loading buffer and heated at 95°C for 5 min. Samples were
631 loaded into pre-cast polyacrylamide gels (4-20% gradient, Bio-Rad) and electrophoresed at 90 V
632 for 1.5 h. Proteins were transferred to 0.45 µm nitrocellulose membranes at 100 V for 1 h.
633 Membranes were blocked in Intercept blocking buffer (LI-COR) for 30 min at room temperature
634 with gentle agitation. Blocking solution was replaced with primary antibody (Spike, LRRC15)
635 Intercept buffer and membranes incubated overnight at 4°C with gentle agitation. Membranes were
636 washed three times with TBST for 5 min with agitation prior to the incubation of membranes with
637 secondary antibody in Intercept buffer for 2 h at room temperature. Membranes were washed
638 another three times with TBST and then imaged using the Odyssey CLx (LICOR).
639
640 **Confocal imaging of cultured cells**
641 13 mm round coverslips were coated with Matrigel (Corning) diluted in DPBS and incubated for
642 30 min at 37°C. HEK293T cells transfected with *LRRC15* cDNA constructs were seeded onto the
643 Matrigel-coated coverslips at a density of 50,000 cells per coverslip. The following day, cells were
644 incubated with Alexa Fluor™ 647-conjugated SARS-CoV-2 spike protein at a concentration of 10
645 µg/mL in culture media for 30 min at 37°C. The cells were fixed in 4% paraformaldehyde (PFA)
646 for 20 min at room temperature, washed 3 times with DPBS. Cells were incubated with Hoechst
647 (1:2000 in DPBS) for 20 minutes, washed 3 times and mounted onto Superfrost plus slides
648 (Fisherbrand) and then imaged using the Leica TCS SP8 STED 3X at 40X magnification.
649

650 **Patients**

651 Post-mortem formalin-fixed paraffin embedded (FFPE) tissue samples were obtained from 4
652 patients who died from severe COVID-19 infection and diagnosed using a PCR test between
653 December 2020 and March 2021. The control group consisted of post-mortem FFPE lung tissue
654 samples from 3 patients with melanoma metastases in the lung. Lung tissue from COVID-19
655 patients was compared with non-tumor lung tissue from melanoma patients. All patients gave
656 informed consent for study participation and the study was performed in accordance with the
657 Declaration of Helsinki guidelines. The study was approved by the Ethics Committee of Eastern
658 Switzerland (BASEC Nr. 2020-01006/EKOS 20/71 and BASEC Nr. 2016-00998/EKOS 16/015).
659

660 **Hematoxylin and Eosin (H&E) staining, LRRC15 and collagen I immunofluorescence (IF)**

661 Post-mortem lung tissue samples were collected and processed for paraffin embedding according
662 to standard diagnostic protocols in the Institute for Pathology of St. Gallen Cantonal Hospital. All
663 tissue samples were routinely stained for histopathological diagnosis with H&E following a
664 standardized validated protocol. Two-micron-thick sections were cut using a Leica RM2255 rotary
665 microtome (Leica Microsystems, DE) and placed on poly-L-lysine-coated slides. Slides were
666 dewaxed in xylene, rehydrated, and subjected to heat-induced epitope retrieval in a sodium citrate
667 solution (pH 6) for 20 minutes in a microwave oven. Slides were then allowed to cool to room
668 temperature followed by a 60-minute incubation with 1x PBS/5% skim milk at RT. Excess liquid
669 was removed and sections were incubated for 18 h at 4°C with a polyclonal rabbit anti-human
670 LRRC15 antibody (LSBio, catalog number LS-C405127, lot ID 134873, dilution 1:50) in 1x PBS.
671 This step was followed by a 1 h incubation at RT with an Alexa Fluor 488 donkey anti-rabbit IgG
672 (H+L) antibody (Jackson Immunoresearch, catalog number 711-545-152, dilution 1:200) in 1x

673 PBS, and another incubation for 2 h at RT with a monoclonal mouse anti-human collagen I
674 antibody (Abcam, catalog number ab88147, clone 3G3, dilution 1:100) labelled with an Alexa
675 Fluor 647 antibody labeling kit (Invitrogen, catalog number A20186) following the manufacturer's
676 instructions. Slides were then counterstained with DAPI, and mounted using fluorescence
677 mounting medium (Dako, Cat. No. S3023).
678
679 **Image acquisition for stained lung tissue samples**
680 Whole slide scans of H&E-stained slides were acquired with a Pannoramic 250 Flash III digital
681 slide scanner (3D Histech, HU). All micrographs from the IF stain were acquired using an LSM980
682 confocal microscope with Airyscan 2 (Zeiss, DE).
683
684 **Generation of TurboGFP-only and TurboGFP-tagged LRRC15 cDNA overexpression lines**
685 VELOCITY DNA Polymerase was used in PCR to generate amplicons containing cDNA for
686 *TurboGFP*-tagged *LRRC15* Transcript 1 (from Origene plasmid RG225990) and *TurboGFP*
687 control. PCR was similarly used to amplify all components from the LentiCRISPR-v2 plasmid
688 with the exception of the *U6-sgRNA* sequence and *Cas9* protein coding sequence. NEBuilder HiFi
689 DNA Assembly Master Mix was used to assemble lentiviral *LRRC15-TurboGFP* and *TurboGFP*-
690 only cDNA constructs using the cDNA amplicons as inserts and LentiCRISPR-v2 fragment as the
691 vector backbone. Assembly products were transformed into 10-beta cells via heat shock, plated
692 onto agarose containing ampicillin at a concentration of 100 µg/mL and incubated for approx. 16
693 h at 37°C. Individual colonies were picked, expanded in Luria broth (Life Technologies)
694 supplemented with ampicillin and amplified constructs were harvested using ISOLATE II Plasmid
695 Mini Kit (Bioline). Successful construct assembly was confirmed via Sanger Sequencing.

696 Lentivirus production and transduction of IMR90 fibroblasts and HEK293T-*ACE2-TMPRSS2*
697 cells was carried out as previously described. Cells were then selected on puromycin at a
698 concentration of 2 μg/mL for a minimum of 72 h and functional cDNA expression confirmed by
699 observation of fluorescence.
700
701 **SARS-CoV-2 pseudotyped lentivirus production and infection assay**
702 SARS-CoV-2 pseudovirus was produced using a five-component plasmid system. Plasmid
703 encoding the SARS-CoV-2 spike protein with an 18 amino acid truncation of the C-terminus or
704 the Delta variant of the SARS-CoV-2 Spike protein was co-transfected into HEK293T cells with
705 pBCKS(HIV-1SDmCMBeGFP-P2A-luc2pre-IIU), which permits equimolar expression of firefly
706 luciferase and EGFP, and packaging plasmids pHCMVgagpolmllstwhv, pcDNA3.1tat101ml and
707 pHCMVRevmlwhvpre. Transfection was carried out using Lipofectamine 3000 Transfection
708 Reagent (ThermoScientific) according to manufacturer's instructions. 16 h after transfection, a
709 media change was performed. Viral media was collected the following day, passed through a 0.45
710 μm filter and then concentrated using 100K MWCO Pierce Protein Concentrators (Life
711 Technologies Australia). Concentrated virus was then stored at -80°C. Pseudovirus particle
712 concentrations were determined using the QuickTiter™ Lentivirus Titer Kit (Cell Biolabs, Inc)
713 under manufacturer conditions.
714
715 For infection of cells with SARS-CoV-2 pseudovirus in *cis* inhibition assays, WT HEK293T,
716 HEK293T-*ACE2* and HEK293T-*ACE2-TMPRSS2* cells were transfected with cDNA for *myc-*
717 *DDK*-tagged *LRRC15* transcript 1 or a control plasmid (lentiGuide-Puro; Addgene #52963). Cells
718 were seeded in 96-well plates, concentrated pseudovirus was added 24 hours later in the presence

719 of 8 μg/ml Polybrene. Successful transduction of cells was confirmed by observing GFP
720 expression 48 h post-tranduction. The extent of transduction was quantified with the Steady-Glo
721 Luciferase Assay System (Promega Corporation) according to the manufacturer's instructions.
722 Briefly, plates were allowed to equilibrate to room temperature before 50 μL of Steady-Glo reagent
723 was added to each well containing 50μL of cell culture media. Plates were incubated at room
724 temperature for 1 h to permit cell lysis and luminescence was then measured using a plate reader.
725 Luminescence of the *LRRC15* cDNA- and control plasmid-transfected cells was normalized to the
726 luminescence values for control cells infected at corresponding viral concentration / pseudovirus
727 number.
728
729 **SARS-CoV-2 authentic virus infection assays**
730 For assessing the inhibitory effect of native overexpression of LRRC15, HEK293T-*ACE2-*
731 *TMPRSS2* cells were transfected with *myc-DDK*-tagged *LRRC15* transcript 1 plasmid (Origene,
732 RC225990) for transient overexpression, with empty *myc-DDK* plasmid as a control plasmid.
733 HEK293T-*ACE2-TMPRSS2* cells were seeded in 384-well plates at a density of 8×10^3 cells/well
734 in the presence of NucBlue™ live nuclear dye (Invitrogen, USA) at a final concentration of 2.5%
735 v/v. The SARS-CoV-2 isolates (Wuhan) were serially diluted in cell-culture medium and an equal
736 volume was then added to the pre-plated and nuclear-stained cells to obtain the desired MOI doses.
737 Viral dilutions were performed in duplicate. Plates were then incubated at 37°C for 48 hours before
738 whole wells were imaged with an IN Cell Analyzer HS2500 high-content microscopy system
739 (Cytiva). Nuclei counts were obtained with automated IN Carta Image Analysis Software (Cytiva)
740 to determine the percentage of surviving cells compared to uninfected controls. *LRRC15* and

741 control plasmid-transfected cells were normalized to the average cell count of uninfected wells for
742 the corresponding cell type to determine the extent of normalized cell death.
743
744 **Single cell RNA-sequencing analysis**
745 *LRRC15* expression was first queried on the COVID-19 cell atlas interactive website and
746 summarized in **Fig. 5a**. In depth analysis of lung single cell datasets were conducted on 3 studies[24–
747 26] with Seurat V4.1.0[60]. Two single nucleus RNAseq datasets were downloaded from the Single
748 Cell Portal (Broad Institute, SCP1052 and SCP1219) and one single cell RNAseq dataset from
749 Gene Expression Omnibus (GSE158127). Their accompanying metadata, which includes
750 information such as sample ID, sample status and cluster annotations (cell types), were added to
751 Seurat objects using the 'AddMetaData' function. Read counts were normalized using
752 SCTransform, before reanalysis with the standard Seurat workflow of 'RunPCA,'
753 'FindNeighbours,' 'FindClusters,' and 'RunUMAP'. Cluster identities were assigned using
754 published cluster annotations and plots were generated with 'DimPlot' and 'DotPlot'. The number
755 of cells in each cluster from each study was then tabulated. 'Subset' was utilized to create new
756 fibroblast only datasets before generating collagen (*COL1A1*, *COL1A2*, *COL8A1*, *COL11A1*,
757 *COL12A1*) dotplots for *LRRC15*-expressing (*LRRC15*>0, Pos) and non-expressing (*LRRC15* = 0,
758 Neg) fibroblasts.
759
760 **Fibroblast infectivity and SARS-CoV-2 pseudovirus co-culture assay**
761 *LRRC15* expression in IMR90 lung fibroblasts were first compared with HEK293T cells by RT-
762 qPCR. These cells were then transfected with empty *TurboGFP* control and *LRRC15-TurboGFP*
763 (Lipofectamine LTX with plus reagent (ThermoScientific)). Cells were checked for Spike binding

764 activity by incubation with Spike647 and detection via flow cytometry 24 h post-transduction.
765 Then, these fibroblasts were infected with SARS-CoV-2 pseudovirus as described above and
766 luciferase luminescence were compared to HEK293T-*ACE2*-*TMPRSS2* cells.
767
768 For SARS-CoV-2 pseudovirus co-culture assay, IMR90 fibroblasts stably over-expressing either
769 *TurboGFP*-alone or *TurboGFP*-tagged *LRRC15* Transcript 1 were mixed with HEK293T-*ACE2*-
770 *TMPRSS2* in a ratio of 2:1 and then seeded at a density of 18,000 cells per well in 96-well plates.
771 SARS-CoV-2 pseudovirus was added to cells the following day in fresh media containing 8 ug/mL
772 Polybrene. Extent of transduction was quantified approximately 16 h later using the Steady-Glo
773 Luciferase Assay System (Promega Corporation) as previously described.
774
775 **Authentic SARS-CoV-2 Virus Bioassay of co-cultured cells**
776 For assessing virus infectivity in the presence of native LRRC15 over-expression, co-culture
777 conditions were established by mixing IMR90 fibroblasts that stably over-expressed *TurboGFP*-
778 tagged *LRRC15* transcript 1 or *TurboGFP*-only with HEK293T-*ACE2*-*TMPRSS2* at a ratio of 2:1.
779 The cell suspensions were seeded on 96-well plates at a density of 18000 cells per well. SARS-
780 CoV-2 isolates (Wuhan) were serially diluted in culture medium and an equal volume was added
781 to seeded cells. Plates were incubated for 24 h at 37°C, and the media was collected and diluted
782 1:10. This media was added using equal volumes in an infection bioassay consisting of
783 hyperpermissive HEK293T-*ACE2*-*TMPRSS2* cells that were seeded in 384-well plates (3000
784 cells/well). Plates were incubated for 72 h at 37°C, and NucBlueTM live nuclear dye (Invitrogen,
785 USA) at a final concentration of 2.5% was added. After a 4 h incubation plates were imaged using
786 an IN Cell Analyzer HS2500 high-content microscopy system (Cytiva). Quantification of nuclei

787 was performed with automated IN Carta Image Analysis Software and normalised to uninfected
788 wells.
789
790 **RNA Sequencing**
791 Total RNA was extracted from IMR90 fibroblasts overexpressing *TurboGFP* alone or *TurboGFP*-
792 tagged *LRRC15* Transcript 1 using the ISOLATE II RNA Mini Kit (Bioline) and quantified via
793 Qubit. 200 ng of each sample was processed with the Illumina Stranded mRNA Prep kit and
794 indexes added with the IDT for Illumina RNA UD Indexes Set A. The prepared libraries were
795 quantified via Qubit and then pooled at a final concentration of 750 pM. PhiX was spiked in at 2%
796 and the pooled libraries were then sequenced on the Illumina NextSeq 2000.
797
798 **Differential Gene Expression Analysis and Ingenuity Pathway Analysis**
799 Differential gene expression analysis was performed using Illumina BaseSpace. Briefly, the BCL
800 Convert app (v2.1.0) was used to generate fastq files from the sequencing run. The DRAGEN
801 FASTQ Toolkit app (v1.0.0) was used to trim adapter sequences and the 5' T-overhang generated
802 during adapter ligation. DRAGEN FastQC + MultiQC (v3.9.5) was used for quality control checks.
803 DRAGEN RNA (v3.10.4) was used for read counting with hg38 Alt-Masked v2, Graph Enabled
804 used as the reference genome. Finally, DRAGEN Differential Expression (v3.10.5) was used for
805 differential gene expression analysis. Output can be found in **Supplementary Table 5**. Output of
806 this differential gene expression analysis was uploaded to Ingenuity (v01-21-03) and filtered such
807 that only genes with adjusted p-value < 0.05 were used in core analysis. Canonical pathway
808 analysis output can be found in **Supplementary Table 6.** Canonical pathways that had a Z-score
809 of 0 or no activity pattern available were disregarded.

810

811 **Quantification and statistical analysis**

812 SARS-CoV-2 spike glycoprotein titration experiments were analyzed on GraphPad Prism and
813 fitted with non-linear regression (one site -- specific binding) to identify maximal binding (B_{max})
814 and dissociation constants (K_D). CRISPR activation screen analysis was performed using
815 MAGeCK (v0.5.9.2)[7]. For each sample, Z-scores were calculated using normalized read counts.
816 Volcano plots were generated using the EnhancedVolcano package for R. All other plots were
817 generated using ggplot2 or GraphPad Prism. All flow cytometry data was analyzed using FlowJo.
818 All RT-qPCR results were analysed using $\Delta\Delta C_T$ method. For *LRRC15* and *COL1A1* RT-qPCR in
819 TGFβ-treated cells, *LRRC15* and *COL1A1* expression in each sample was normalised to
820 expression in untreated cells. Significance was assessed with Mann-Whitney One Tailed t-test. For
821 SARS-CoV-2 pseudovirus and live virus experiments, data shown reflects ≥3 independent
822 replicates. For pseudovirus experiments in monocultures, results are reported as either raw
823 luminescence values or as normalized level of transduction, calculated by dividing luminescence
824 recorded for LRRC15-transfected cells by luminescence relative to control. For pseudovirus co-
825 culture experiments, normalized level of transduction was calculated by dividing luminescence
826 recorded for LRRC15 expressing cells by control cells transduced at the same number of
827 pseudovirus particles. For authentic virus monoculture and co-culture infection assays, cell death
828 for both control and LRRC15-transfected cells was normalized to uninfected cells of the same line.
829 Significance for SARS-CoV-2 pseudotyped lentivirus and authentic virus experiments were
830 analyzed with two-way ANOVA with Sidak Multiple Comparisons test. For analysis of pooled
831 independent single cell/nuc sequencing datasets, significance was assessed using unpaired t-test.
832 Significance of differentially expressed genes was assessed using the DRAGEN Differential

833 Expression application, which utilizes DESeq2. Z-score for DEG canonical pathways was
834 determined by Ingenuity. For RT-qPCR confirmation of upregulated antiviral gene signature and
835 downregulated collagen gene signature, expression was normalized to the average of the control
836 GFP cells and significance was assessed using One-Tailed Mann-Whitney tests. All error bars in
837 this manuscript report SEM unless otherwise stated.
838

839 **Acknowledgements**
840 We thank Novogene for CRISPRa library sequencing, Sydney Informatics Hub (Artemis HPC)
841 for single cell data analysis infrastructure, Sydney Cytometry for flow cytometry and FACS
842 support, the technical and scientific assistance of Sydney Microscopy & Microanalysis, the
843 University of Sydney node of Microscopy Australia, Dr Megan Steain, Dr Mark Larance, Dr Sean
844 Humphrey, Dr Gang Liu, Dr Phil Hansboro, Dr Tim Newsome and members of the Neely lab for
845 helpful discussions. Figure illustrations were created with BioRender.com.
846

847 **Funding**
848 G.N. is funded by the National Health and Medical Research Council (NHMRC) project grants
849 APP1107514, APP1158164, APP1158165, the NSW Ministry of Health, and a philanthropic
850 donation from Dr. John and Anne Chong. L.L. is funded by a Dr. John and Anne Chong Fellowship
851 for Genome Editing and seed funding from the Drug Discovery Initiative at the University of
852 Sydney. L.F. is supported by the Swiss National Science foundation grant PP00P3_157448.
853 O.H.A. is funded by a Swiss National Science Foundation fellowship no. P400PM_194473..
854

855 **Author contributions**

LL, GGN conceived this project. LL, FC established the CRISPRa system. MW validated the efficiency of the CRISPRa system. LL, MW performed whole genome screening and target validation. LL, AJC performed pseudolentivirus *Cis* experiments with input from DH. CLM performed microscopy of cultured cells. LL performed western blots. AJ, OHA, and OTP designed, performed, and analysed human lung histology. MW, CED performed molecular cloning. AA generated ACE2 and ACE2-TMPRSS2 cell lines. MW generated stable overexpression lines and carried out RNA sequencing analysis. MW, ZH performed RT-qPCR. JKKL, KP, RS, JM produced Spike protein. CLM, ST, AJC, DH, TK, and SM helped with SARS-CoV-2 neutralization studies. LL, MW, AJC, CLM, AOS, DH, GGN performed data analyses. LL, LF, DH, ST, GGN provided supervision and project administration. LL, MW, GGN wrote the manuscript with contributions from all authors.

Declaration of interests

The authors declare no competing interests.

872 **Figure Legends**

873

874 **Figure 1. A sensitive FACS-based SARS-CoV-2 Spike binding assay amenable to high**
875 **throughput screening.**

876 **a** Schematic of SARS-CoV-2 Spike binding assay. HEK293T cells with stable integration of *ACE2*
877 cDNA for overexpression (HEK293T-*ACE2*) are incubated with Alexa Fluor 488-conjugated
878 SARS-CoV-2 Spike protein (Spike488). Spike488-binding cells are then detected by flow
879 cytometry. **b** Representative flow cytometry plots for *WT* HEK293T and HEK293T-*ACE2*
880 incubated with Spike488 (N=3). See also **Supplementary Fig. 1b** for gating strategy. **c** Titration
881 of HEK293T-*ACE2* (*ACE2*) cells with *WT* HEK293T cells. 1% HEK293T-*ACE2* cells showed a
882 difference to baseline non-specific binding. Histogram summary showing mean fluorescence
883 intensity (MFI) of flowed cells. **d** Schematic of CRISPR activation (CRISPRa) system used. **e**
884 Representative plot of flow cytometry for a clonal HEK293T-CRISPRa cell line transduced with
885 NTC sgRNA or *ACE2* sgRNA (expression confirmation via RT-qPCR in **Supplementary Fig.**
886 **1a**).

887

888 **Figure 2. Whole genome CRISPRa screening identified LRRC15 as a novel SARS-CoV-2**
889 **Spike-binding protein.**

890 **a** Schematic of CRISPRa screen used to identify regulators of SARS-CoV-2 Spike-binding. **b**
891 Ranking of all genes in screen 1 by $\log_2$ fold change calculated using MAGeCK and plotted using
892 MAGeCKFlute. See also **Supplementary Table 1**. **c** Gene enrichment analysis of screen 1
893 performed using MAGeCK. Horizontal dotted line indicates p-value = 0.05. Vertical dotted line
894 indicates $\log_2$ fold changes (LFCs) of 2. P-values and LFCs for all genes are reported in

895 **Supplementary Table 1**. **d** sgRNA Z-scores for screen 1 unsorted and sorted samples. Density
896 curve for all sgRNA Z-scores in sample (i.e. sorted or unsorted) is shown in grey. Z-scores for
897 each guide are indicated by vertical lines (blue ACE2, red LRRC15). **e** Flow cytometry analysis
898 of HEK293T-CRISPRa cells transduced with three independent *LRRC15* sgRNAs. HEK293T-
899 CRISPRa transduced with *ACE2* sgRNA3 were used as a positive control and NTC sgRNA-
900 transduced HEK293T-CRISPRa cells were used as a negative control (N = 3). **f** Quantification of
901 Spike647 binding in *ACE2* sgRNA3 and *LRRC15* sgRNA1 cells via flow cytometry. Dissociation
902 constant (Kd) was calculated by fitting with non-linear regression (one site -- specific binding). N
903 = 3, error bars represent S.D.
904
905 **Figure 3. Confirmation that LRRC15 binds to SARS-CoV-2 Spike protein.**
906 **a** LRRC15 contains 15 leucine-rich repeats, a short cytoplasmic C-terminus, and 2 glycosylation
907 sites. **b** Predicted protein structure of LRRC15 (from alpha fold). **c** LRRC15 is part of the LRR-
908 Tollkin family. **d** Flow cytometry analysis of Alexa Fluor-647 (Spike647) binding in WT
909 HEK293T cells, **e** HEK293T-*ACE2* and **f** HEK293T cells with stable expression of *ACE2* cDNA
910 and *TMPRSS2* cDNA (HEK293T-*ACE2-TMPRSS2*). Each cell line was transfected with plasmids
911 encoding cDNA for *GFP*-tagged *LRRC15* (transcript 1 or 2) or with empty *GFP* vector as negative
912 control plasmid. **g**. Histogram summary shows mean fluorescence intensity (MFI) of **d-f**. **h**
913 Representative images of interaction between LRRC15-GFP and Alexa Fluor 647-conjugated
914 SARS-CoV-2 HexaPro Spike protein in HEK293T cells (N = 2). Images were taken at 40x
915 magnification. Green = LRRC15-GFP, Red = Spike647, Blue = Hoechst-stained nuclei. Scale bar
916 = 25 μm. **i** Immunoprecipitation of LRRC15 with Spike protein. Lysates of HEK293T cells
917 transfected with GFP-tagged *LRRC15* (transcript 1 or 2, *LRRC15_1* and *LRRC15_2*, respectively)

incubated with SARS-CoV-2 HexaPro Spike protein were immunoprecipitated using anti-LRRC15 primary antibody. Immunoblots were performed for LRRC15 and for SARS-CoV-2 HexaPro spike. I = input, FT = flow-through, E = elute.

Figure 4. LRRC15 is expressed in lung fibroblasts and lines the airways in COVID-19 patients.

a Overview of cell types expressing *LRRC15* from existing single cell RNA-sequencing datasets. **b** UMAP plot of lung single nucleus RNAseq dataset (Melms et al). **c** Feature plot and **d** Dotplot shows *LRRC15* is expressed in fibroblasts and neuronal cells. Expression of *LRRC15* is also observed in fibroblasts of separate studies (See **Supplementary Fig. 5**). **e** Proportion of cells that are lung fibroblasts increases with COVID lungs (7.9% in control (N = 19) and 22.9% in COVID (N = 47); Unpaired t test, $p<0.0001$) **f-g** Representative micrograph of hematoxylin and eosin (H&E) stained lung tissue section obtained from **f** a human donor without COVID-19 and **g** donor diagnosed with COVID-19. Imaging performed at 200x magnification (Scale bar = 50 m). All images in **Supplementary Fig. 6a** (Control, N = 1; COVID-19, N = 4). **h-i** Representative micrograph of immunofluorescence staining in human lung tissue section obtained from **h** donor without COVID-19 and **i** donor diagnosed with COVID-19. Images were taken at 200x magnification (Scale bar = 100 m). Red = Collagen I, green = LRRC15, blue = DAPI. All images in **Supplementary Fig. 6b** (Control, N = 3; COVID-19, N = 4).

Figure 5. LRRC15 is not a SARS-CoV-2 entry receptor but inhibits infection in *trans.*

a IMR90 fibroblasts express *LRRC15*, quantified via RT-qPCR. N=3 per cell line. **b-c** TGFβ increased **b** *LRRC15* and **c** *COL1A1* in fibroblasts, quantified via RT-qPCR. N = 7 for each group.

941 Significance was determined by Mann-Whitney One-Tailed test, **p<0.01. **d** IMR90 fibroblasts
942 expressing *LRRC15* bind spike, MFI = Mean Fluorescence Intensity. **e** Fibroblasts do not have
943 innate tropism for SARS-CoV-2 and overexpression of *LRRC15* does not mediate infection.
944 Transduction efficiency (luciferase luminescence) was compared to permissive cell line
945 HEK293T-*ACE2-TMPRSS2*. N = 2 independent replicates for each group. **f** Pooled analysis of 3
946 independent studies indicate ratio of fibroblasts to epithelial cells in COVID lungs is approx. 2:1
947 (0.3 in control (n=19) and 2.06 in COVID (n=47); Unpaired two-tailed t test, p<0.0001). **g**
948 LRRC15 expressing fibroblasts can suppress SARS-CoV-2 spike pseudovirus infection of
949 HEK293T-*ACE2-TMPRSS2* cells. Significance was determined by two-way ANOVA, Sidak's
950 multiple comparison test, **p<0.01,*p<0.05. N = 6 per condition. **h** LRRC15 expressing
951 fibroblasts can suppress authentic SARS-CoV-2 infection of HEK293T-*ACE2-TMPRSS2* cells.
952 Significance was determined by two-way ANOVA, Sidak's multiple comparison test, *p<0.05. N
953 = 3 per condition.
954
955 **Figure 6. LRRC15 expression is correlated with collagen and antiviral gene signatures.**
956 **a** *LRRC15*$^{+}$ fibroblasts have an enhanced collagen gene signature. Dotplots generated from 3
957 separate studies. Pos = *LRRC15*$^{+}$, Neg = *LRRC15*$^{-}$. **b** Volcano plot of differentially expressed genes
958 (DEGs) from fibroblasts ectopically expressing either LRRC15 or GFP. N = 3 biological replicates
959 for each group. A subset of DEGs is labelled, including collagen genes and genes related to
960 antiviral signaling. Blue labels indicate downregulation while red labels indicate upregulation. **c**
961 DEG-associated canonical pathways as determined by Ingenuity Pathway Analysis. Canonical
962 pathways were filtered to show only those with p-value < 0.05 and with a nonzero Z-score (i.e.,
963 pathways that had no activity pattern or a Z-score of 0 are not shown). **d-e** *LRRC15* overexpression

964 causes **d** upregulation of antiviral transcripts and **e** downregulation of collagen transcripts by RT-
965 qPCR. Results were calculated using the $\Delta\Delta C_T$ method, normalized to the average of control *GFP*-
966 only cells. Significance was assessed using one-tailed Mann Whitney test, *$p<0.05$. N = 3 per
967 condition. **f** Ectopic expression of LRRC15 in fibroblasts decreases Collagen VI protein expression
968 compared to *GFP*-only control cells. Western blots for LRRC15 and Collagen VI.
969
970
971 **Supplementary Fig. 1. CRISPR activation screen setup.**
972 **a** RT-qPCR of *ACE2* expression in SAM clonal cell lines transduced with *ACE2* sgRNAs, or with
973 HEK293T-*ACE2* cells. Results calculated using $\Delta\Delta C_T$ method and normalized to non-targeting
974 control (NTC) sgRNA-transduced HEK293T-CRISPRa cells. **b** FACS gating strategy. Cells were
975 first gated by forward (FSC) and side scatter (SSC) before filtering for singlets. Spike488
976 fluorescence was gated by comparison with non-targeting control (NTC) sgRNA transduced cells.
977 Similar strategy was applied to all flow cytometry experiments. **c** FACS results for 3 whole
978 genome CRISPRa screens with NTC sgRNA-transduced cells as negative controls. For screen 1,
979 cells were incubated with Alexa Fluor 488-conjugated SARS-CoV-2 HexaPro Spike (Addgene
980 #154754) and selected on puromycin for 3 days. For screen 2, cells were incubated with Alexa
981 Fluor 488-conjugated SARS-CoV-2 Spike glycoprotein (residues 1-1208, complete ectodomain;
982 gift from Dr. Florian Krammer) and selected on puromycin for 3 days. For screen 3, cells were
983 incubated with Alexa Fluor 488-conjugated SARS-CoV-2 HexaPro spike (Addgene #15474) and
984 selected on puromycin for 8 days.
985
986 **Supplementary Fig. 2. CRISPR screen analysis and validation.**

987 **a-b** Gene enrichment analysis of screens 2 (A) and 3 (B) performed using MAGeCK. Horizontal
988 dotted line indicates p-value = 0.05. Vertical dotted line indicates log_2 fold changes (LFCs) of 2.
989 P-values and LFCs for all genes in screens 2 and 3 are reported in **Supplementary Table 1. c-d**
990 Density plot of Z-score (grey) for all sgRNA in (C) screen 2 and (D) screen 3. Blue vertical lines
991 indicate Z-score for *ACE2* sgRNAs. Red vertical lines indicate Z-score for *LRRC15* sgRNAs. Z-
992 scores calculated as described in methods. **e** Log_2 fold changes of all genes in Screen 1 vs. log_2
993 fold changes of all genes in Screen 2. **f** Log_2 fold changes of all genes in Screen 1 vs. log_2 fold
994 changes of all genes in Screen 3. **g** *LRRC15* expression of cells in Fig 2e quantified via RT-qPCR.
995 **h** *ACE2* expression was not increased in *LRRC15* sgRNA transduced cells (quantified via RT-
996 qPCR). **i** The 3 sgRNAs for *ACE2* from the Calabrese library used in our screens were transduced
997 into HEK293T-CRISPRa cells and *ACE2* expression was confirmed via qPCR. Only sgRNA3
998 induced upregulation in *ACE2* expression. **j** Transduced cells in **i** were incubated with Spike647
999 and analysed via flow cytometry. Only *ACE2* sgRNA3 cells showed a significant increase in
1000 Spike647 binding.
1001
1002 **Supplementary Fig 3. LRRC15 is related to TLRs and interacts with Spike.**
1003 **a** Full phylogenetic tree of LRR-Tollkin family of proteins (includes fly and worm orthologs).
1004 **b** Co-immunoprecipitation of Spike was observed in LRRC15-GFP (transcripts 1 and 2) and ACE2
1005 expressing cells but not in control GFP cells. I = input, FT = flow-through, E = elute. **c** Control
1006 rabbit IgG did not immunoprecipitate LRRC15 or Spike.
1007
1008 **Supplementary Fig 4. LRRC15 expression inhibits SARS-CoV-2 Spike pseudovirus infection**
1009 **in ACE2 expressing cells. a** SARS-CoV-2 pseudovirus carrying a firefly luciferase cassette was

1010 applied to HEK293T, HEK293T-*ACE2* and HEK293T-*ACE2-TMPRSS2* cells for 24 hours before
1011 luminescence quantification. HEK293T cells were relatively resistant to infection while
1012 HEK293T-*ACE2* and HEK293T-*ACE2-TMPRSS2* expressing cells were infectable. N=3 for each
1013 condition. **b** Pseudovirus added to ACE2-expressing cells in the context of LRRC15. Titration of
1014 $15x10^6$, $62.5x10^6$, $250x10^6$ and $1000x10^6$ lentiviral particles in HEK293T-*ACE2* cells transfected
1015 with 0, 156.25, 312.5, 625, 1250 and 2500 ng of *Myc-DDK-tagged LRRC15* plasmid DNA. N=2
1016 for each condition. **c-d** Luciferase assay for quantification of SARS-CoV-2 pseudovirus infection
1017 in **c** HEK293T-*ACE2* and **d** HEK293T-*ACE2-TMPRSS2* (N = 3). Cells were transfected with
1018 plasmid encoding *Myc-DDK-tagged LRRC15* transcript 1 or empty vector as a control.
1019 Luminescence for *LRRC15* cells were normalized to control cells. Significance was determined by
1020 two-way ANOVA, Sidak multiple comparison test; ****$p<0.0001$, ***$p<0.001$, **$p<0.01$,
1021 *$p<0.05$.
1022 **e** Quantification of cell survival after incubation with authentic SARS-CoV-2 virus in HEK293T-
1023 *ACE2-TMPRSS2* cells transfected with plasmid encoding *Myc-DDK*-tagged *LRRC15* transcript 1
1024 or *Myc-DDK* only (N = 3). Significance was determined by two-way ANOVA, *$p<0.05$.
1025
1026 **Supplementary Fig 5. Single cell/nucleus analysis of different studies corroborates restricted**
1027 ***LRRC15* expression in fibroblasts.**
1028 **a** UMAP plot of lung single nucleus RNAseq dataset (Delorey et al). **b** Feature plot and **c** Dotplot
1029 shows *LRRC15* is expressed in Delorey et al. fibroblasts. **d** UMAP plot of lung single nucleus
1030 RNAseq dataset (Bharat et al). **e** Feature plot and **f** Dotplot shows *LRRC15* is expressed in Bharat
1031 et al. Lymphatic Endothelial cells and various populations of fibroblasts.
1032

1033 **Supplementary Fig. 6. H&E and immunofluorescence staining of human lung tissue samples**

1034 Representative micrographs of **a** haematoxylin and eosin staining and **b** immunofluorescence
1035 staining of post-mortem formalin-fixed paraffin embedded human lung samples obtained from
1036 donors who died of severe COVID-19. Control samples were obtained from patients with
1037 melanoma metastases in the lung and non-tumor tissue used for comparisons. Micrographs taken
1038 at 200x magnification. Scale bar = 50 μM for **a**, 100 μM for **b**. In **b**, Red = Collagen I, Green =
1039 LRRC15, Blue = DAPI.

1040

1041 **Supplementary Fig. 7. IMR90 fibroblasts bind SARS-CoV-2 Spike and *LRRC15* over-**
1042 **expressing fibroblasts show decreased Collagen VI expression**

1043 **a** Representative flow cytometry analysis of IMR90 fibroblasts incubated with Spike647 show
1044 cells have intrinsic Spike binding activity (N = 2). **b** Full images for LRRC15 and Collagen VI
1045 western blots. *LRRC15* overexpression in fibroblasts results in decreased Collagen VI protein
1046 expression.

1047

1048

1049 **Supplementary Table 1: CRISPR activation screen MAGeCK outputs.**

1050 Collated output of MAGeCK and MAGeCKFlute pipeline. For each screen, normalized read
1051 counts and Z-scores, gene-level summary, sgRNA-level summary and output of MAGeCKFlute
1052 ReadRRA() function is provided.

1053

1054 **Supplementary Table 2: Oligonucleotides for CRISPR activation sgRNA constructs**

1055 Lists oligonucleotides used for generation of CRISPRa sgRNA constructs. Sequences for each
1056 sgRNA construct were from either Weismann lab Human Genome-wide CRISPRa-v2 Library
1057 (Addgene, #83978) or Calabrese Library Set A (Addgene, #92379).
1058
1059 **Supplementary Table 3: Next Generation Sequencing Primers**
1060 List of primers used for next generation sequencing of gDNA extracted from pooled CRISPR
1061 activation screen samples. Primers were adapted from Sanson et al. [5].
1062
1063 **Supplementary Table 4: RT-qPCR primer sequences**
1064 List of primers used for RT-qPCR.
1065
1066 **Supplementary Table 5: Differential Gene Expression Analysis Results**
1067 Output of DRAGEN Differential Expression application.
1068
1069 **Supplementary Table 6**: **Ingenuity Comparison Analysis Canonical Pathways Results.**
1070 Canonical pathways output from Ingenuity Comparison Analysis using DRAGEN Differential
1071 Expression results for IMR90 *TurboGFP* vs. IMR90 *LRRC15 T1-TurboGFP* for input.
1072

1073

1074 **References**

1075

1076 1. Li, W. *et al.* Angiotensin-converting enzyme 2 is a functional receptor for the SARS coronavirus.
1077 *Nature* **426**, 450–454 (2003).
1078 2. Kuba, K. *et al.* A crucial role of angiotensin converting enzyme 2 (ACE2) in SARS coronavirus-
1079 induced lung injury. *Nat. Med.* **11**, 875–879 (2005).
1080 3. Zhou, P. *et al.* A pneumonia outbreak associated with a new coronavirus of probable bat origin.
1081 *Nature* **579**, 270–273 (2020).
1082 4. Lu, R. *et al.* Genomic characterisation and epidemiology of 2019 novel coronavirus: implications for
1083 virus origins and receptor binding. *Lancet* **395**, 565–574 (2020).
1084 5. Sanson, K. R. *et al.* Optimized libraries for CRISPR-Cas9 genetic screens with multiple modalities.
1085 *Nat. Commun.* **9**, 5416 (2018).
1086 6. Horlbeck, M. A. *et al.* Compact and highly active next-generation libraries for CRISPR-mediated
1087 gene repression and activation. *Elife* **5**, (2016).
1088 7. Li, W. *et al.* MAGeCK enables robust identification of essential genes from genome-scale
1089 CRISPR/Cas9 knockout screens. *Genome Biol.* **15**, 554 (2014).
1090 8. Wang, B. *et al.* Integrative analysis of pooled CRISPR genetic screens using MAGeCKFlute. *Nat.*
1091 *Protoc.* **14**, 756–780 (2019).
1092 9. Lan, J. *et al.* Structure of the SARS-CoV-2 spike receptor-binding domain bound to the ACE2
1093 receptor. *Nature* **581**, 215–220 (2020).
1094 10. Wrapp, D. *et al.* Cryo-EM structure of the 2019-nCoV spike in the prefusion conformation. *Science*
1095 **367**, 1260–1263 (2020).
1096 11. Wang, Q. *et al.* Structural and Functional Basis of SARS-CoV-2 Entry by Using Human ACE2. *Cell*
1097 **181**, 894–904.e9 (2020).

1098 12. Dolan, J. *et al.* The extracellular leucine-rich repeat superfamily; a comparative survey and analysis
1099 of evolutionary relationships and expression patterns. *BMC Genomics* **8**, 320 (2007).
1100 13. Hsieh, C.-L. *et al.* Structure-based design of prefusion-stabilized SARS-CoV-2 spikes. *Science* **369**,
1101 1501–1505 (2020).
1102 14. Uhlén, M. *et al.* Proteomics. Tissue-based map of the human proteome. *Science* **347**, 1260419
1103 (2015).
1104 15. Vento-Tormo, R. *et al.* Single-cell reconstruction of the early maternal-fetal interface in humans.
1105 *Nature* **563**, 347–353 (2018).
1106 16. Huang, N. *et al.* SARS-CoV-2 infection of the oral cavity and saliva. *Nat. Med.* **27**, 892–903 (2021).
1107 17. Madissoon, E. *et al.* scRNA-seq assessment of the human lung, spleen, and esophagus tissue stability
1108 after cold preservation. *Genome Biol.* **21**, 1 (2019).
1109 18. Park, J.-E. *et al.* A cell atlas of human thymic development defines T cell repertoire formation.
1110 *Science* **367**, (2020).
1111 19. Martin, J. C. *et al.* Single-Cell Analysis of Crohn's Disease Lesions Identifies a Pathogenic Cellular
1112 Module Associated with Resistance to Anti-TNF Therapy. *Cell* **178**, 1493–1508.e20 (2019).
1113 20. Solé-Boldo, L. *et al.* Single-cell transcriptomes of the human skin reveal age-related loss of
1114 fibroblast priming. *Commun Biol* **3**, 188 (2020).
1115 21. Henry, G. H. *et al.* A Cellular Anatomy of the Normal Adult Human Prostate and Prostatic Urethra.
1116 *Cell Rep.* **25**, 3530–3542.e5 (2018).
1117 22. Vieira Braga, F. A. *et al.* A cellular census of human lungs identifies novel cell states in health and
1118 in asthma. *Nat. Med.* **25**, 1153–1163 (2019).
1119 23. Buechler, M. B. *et al.* Cross-tissue organization of the fibroblast lineage. *Nature* **593**, 575–579
1120 (2021).
1121 24. Delorey, T. M. *et al.* COVID-19 tissue atlases reveal SARS-CoV-2 pathology and cellular targets.
1122 *Nature* **595**, 107–113 (2021).
1123 25. Bharat, A. *et al.* Lung transplantation for patients with severe COVID-19. *Sci. Transl. Med.* **12**,

1124 (2020).
1125 26. Melms, J. C. *et al.* A molecular single-cell lung atlas of lethal COVID-19. *Nature* **595**, 114–119
1126 (2021).
1127 27. Satoh, K., Hata, M. & Yokota, H. A novel member of the leucine-rich repeat superfamily induced in
1128 rat astrocytes by beta-amyloid. *Biochem. Biophys. Res. Commun.* **290**, 756–762 (2002).
1129 28. Dominguez, C. X. *et al.* Single-Cell RNA Sequencing Reveals Stromal Evolution into LRRC15+
1130 Myofibroblasts as a Determinant of Patient Response to Cancer Immunotherapy. *Cancer Discov.* **10**,
1131 232–253 (2020).
1132 29. Krishnamurty, A. T. *et al.* LRRC15+ myofibroblasts dictate the stromal setpoint to suppress tumour
1133 immunity. *Nature* (2022) doi:10.1038/s41586-022-05272-1.
1134 30. O'Prey, J., Wilkinson, S. & Ryan, K. M. Tumor antigen LRRC15 impedes adenoviral infection:
1135 implications for virus-based cancer therapy. *J. Virol.* **82**, 5933–5939 (2008).
1136 31. Hayashi, F. *et al.* The innate immune response to bacterial flagellin is mediated by Toll-like receptor
1137 5. *Nature* **410**, 1099–1103 (2001).
1138 32. Shilts, J. *et al.* LRRC15 mediates an accessory interaction with the SARS-CoV-2 spike protein.
1139 bioRxiv 2021.09.25.461776; doi: https://doi.org/10.1101/2021.09.25.461776. *bioRxiv*
1140 2021.09.25.461776 (2021) doi:10.1101/2021.09.25.461776.
1141 33. Song, J. *et al.* LRRC15 inhibits SARS-CoV-2 cellular entry in trans. *PLoS Biol.* **20**, e3001805
1142 (2022).
1143 34. Loo, L. *et al.* LRRC15 suppresses SARS-CoV-2 infection and controls collagen production. *bioRxiv*
1144 2021.11.09.467981 (2021) doi:10.1101/2021.11.09.467981.
1145 35. Zhu, S. *et al.* Genome-wide CRISPR activation screen identifies candidate receptors for SARS-CoV-
1146 2 entry. *Sci. China Life Sci.* (2021) doi:10.1007/s11427-021-1990-5.
1147 36. Schneider, W. M. *et al.* Genome-Scale Identification of SARS-CoV-2 and Pan-coronavirus Host
1148 Factor Networks. *Cell* **184**, 120–132.e14 (2021).
1149 37. Baggen, J. *et al.* Genome-wide CRISPR screening identifies TMEM106B as a proviral host factor

1150 for SARS-CoV-2. *Nat. Genet.* **53**, 435–444 (2021).

1151 38. Wang, R. *et al.* Genetic Screens Identify Host Factors for SARS-CoV-2 and Common Cold
1152 Coronaviruses. *Cell* **184**, 106–119.e14 (2021).

1153 39. Goujon, C. *et al.* Bidirectional genome-wide CRISPR screens reveal host factors regulating SARS-
1154 CoV-2, MERS-CoV and seasonal HCoVs. *Res Sq* (2021) doi:10.21203/rs.3.rs-555275/v1.

1155 40. Wei, J. *et al.* Genome-wide CRISPR Screens Reveal Host Factors Critical for SARS-CoV-2
1156 Infection. *Cell* **184**, 76–91.e13 (2021).

1157 41. Daniloski, Z. *et al.* Identification of Required Host Factors for SARS-CoV-2 Infection in Human
1158 Cells. *Cell* **184**, 92–105.e16 (2021).

1159 42. Singh, D. K. *et al.* Myeloid cell interferon responses correlate with clearance of SARS-CoV-2. *Nat.*
1160 *Commun.* **13**, 679 (2022).

1161 43. Yoshida, M. *et al.* Local and systemic responses to SARS-CoV-2 infection in children and adults.
1162 *Nature* **602**, 321–327 (2022).

1163 44. Abbas, Y. M., Pichlmair, A., Górna, M. W., Superti-Furga, G. & Nagar, B. Structural basis for viral
1164 5'-PPP-RNA recognition by human IFIT proteins. *Nature* **494**, 60–64 (2013).

1165 45. Schindewolf, C. *et al.* SARS-CoV-2 uses nonstructural protein 16 to evade restriction by IFIT1 and
1166 IFIT3. *bioRxivorg* (2022) doi:10.1101/2022.09.26.509529.

1167 46. Gao, S. *et al.* Structural basis of oligomerization in the stalk region of dynamin-like MxA. *Nature*
1168 **465**, 502–506 (2010).

1169 47. Bizzotto, J. *et al.* SARS-CoV-2 Infection Boosts MX1 Antiviral Effector in COVID-19 Patients.
1170 *iScience* **23**, 101585 (2020).

1171 48. Schroeder, S. *et al.* Interferon antagonism by SARS-CoV-2: a functional study using reverse
1172 genetics. *Lancet Microbe* **2**, e210–e218 (2021).

1173 49. Donovan, J., Dufner, M. & Korennykh, A. Structural basis for cytosolic double-stranded RNA
1174 surveillance by human oligoadenylate synthetase 1. *Proc. Natl. Acad. Sci. U. S. A.* **110**, 1652–1657
1175 (2013).

1176 50. Wickenhagen, A. *et al.* A prenylated dsRNA sensor protects against severe COVID-19. *Science* **374**,
1177 eabj3624 (2021).
1178 51. Gisby, J. S. *et al.* Multi-omics identify LRRC15 as a COVID-19 severity predictor and persistent
1179 pro-thrombotic signals in convalescence. *bioRxiv* (2022) doi:10.1101/2022.04.29.22274267.
1180 52. Rendeiro, A. F. *et al.* The spatial landscape of lung pathology during COVID-19 progression. *Nature*
1181 **593**, 564–569 (2021).
1182 53. Tea, F. *et al.* SARS-CoV-2 neutralizing antibodies: Longevity, breadth, and evasion by emerging
1183 viral variants. *PLoS Med.* **18**, e1003656 (2021).
1184 54. Follenzi, A. *et al.* Targeting lentiviral vector expression to hepatocytes limits transgene-specific
1185 immune response and establishes long-term expression of human antihemophilic factor IX in mice.
1186 *Blood* **103**, 3700–3709 (2004).
1187 55. Aggarwal, A. *et al.* Mobilization of HIV spread by diaphanous 2 dependent filopodia in infected
1188 dendritic cells. *PLoS Pathog.* **8**, e1002762 (2012).
1189 56. Jumper, J. *et al.* Highly accurate protein structure prediction with AlphaFold. *Nature* **596**, 583–589
1190 (2021).
1191 57. UniProt Consortium. UniProt: the universal protein knowledgebase in 2021. *Nucleic Acids Res.* **49**,
1192 D480–D489 (2021).
1193 58. Sievers, F. *et al.* Fast, scalable generation of high-quality protein multiple sequence alignments using
1194 Clustal Omega. *Mol. Syst. Biol.* **7**, 539 (2011).
1195 59. Stecher, G., Tamura, K. & Kumar, S. Molecular Evolutionary Genetics Analysis (MEGA) for
1196 macOS. *Mol. Biol. Evol.* **37**, 1237–1239 (2020).
1197 60. Hao, Y. *et al.* Integrated analysis of multimodal single-cell data. *Cell* **184**, 3573–3587.e29 (2021).

1198

1199

1200

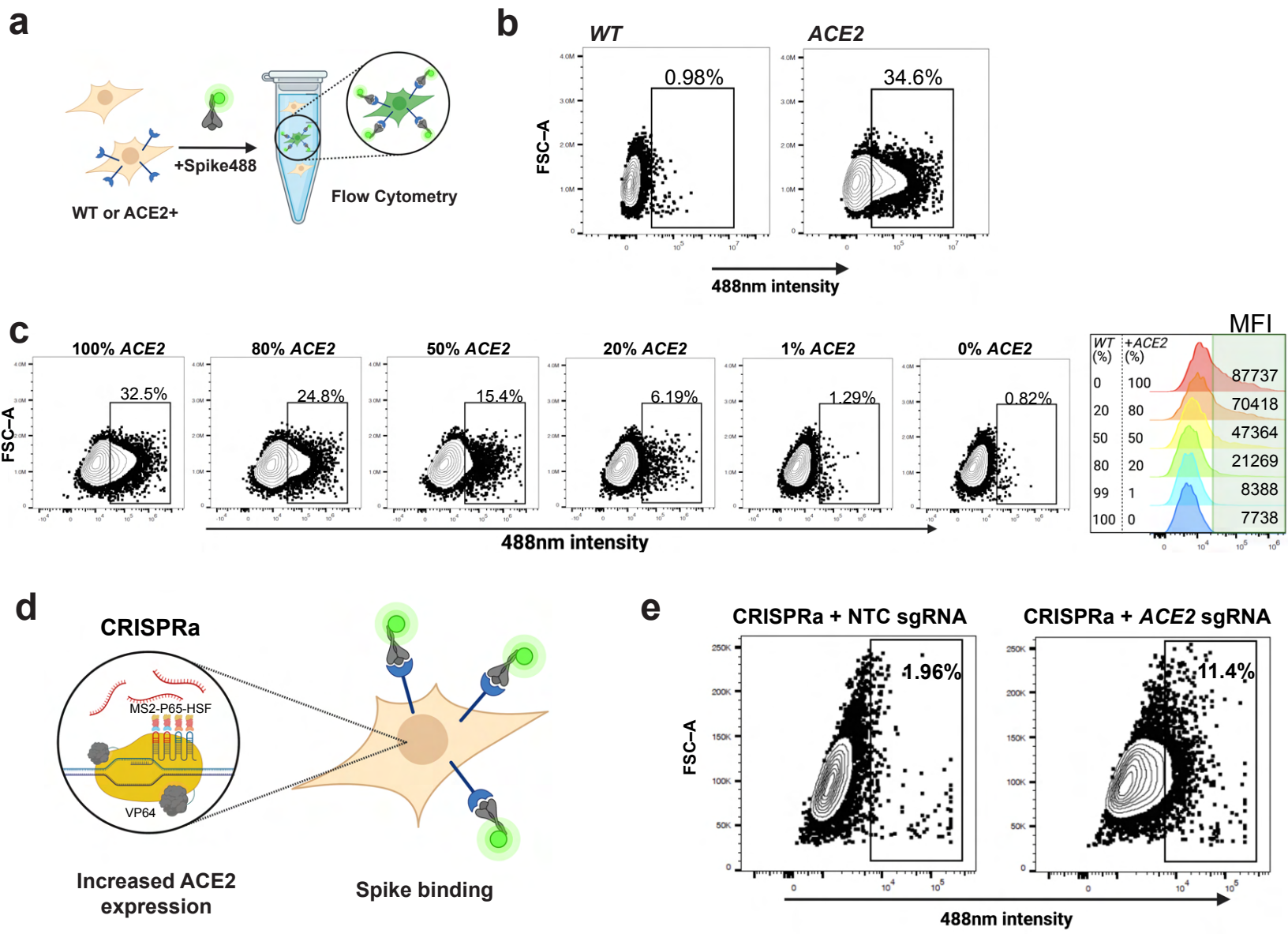
a
WT or ACE2+
+Spike488
Flow Cytometry
b
WT
ACE2
0.98%
34.6%
FSC–A
488nm intensity
c
100% ACE2
80% ACE2
50% ACE2
20% ACE2
1% ACE2
0% ACE2
32.5%
24.8%
15.4%
6.19%
1.29%
0.82%
FSC–A
488nm intensity
MFI
WT (%)
+ACE2 (%)
0 100 87737
20 80 70418
50 50 47364
80 20 21269
99 1 8388
100 0 7738
d
CRISPRa
MS2-P65-HSF
VP64
Increased ACE2 expression
Spike binding
e
CRISPRa + NTC sgRNA
CRISPRa + ACE2 sgRNA
1.96%
11.4%
FSC–A
488nm intensity

Figure 1

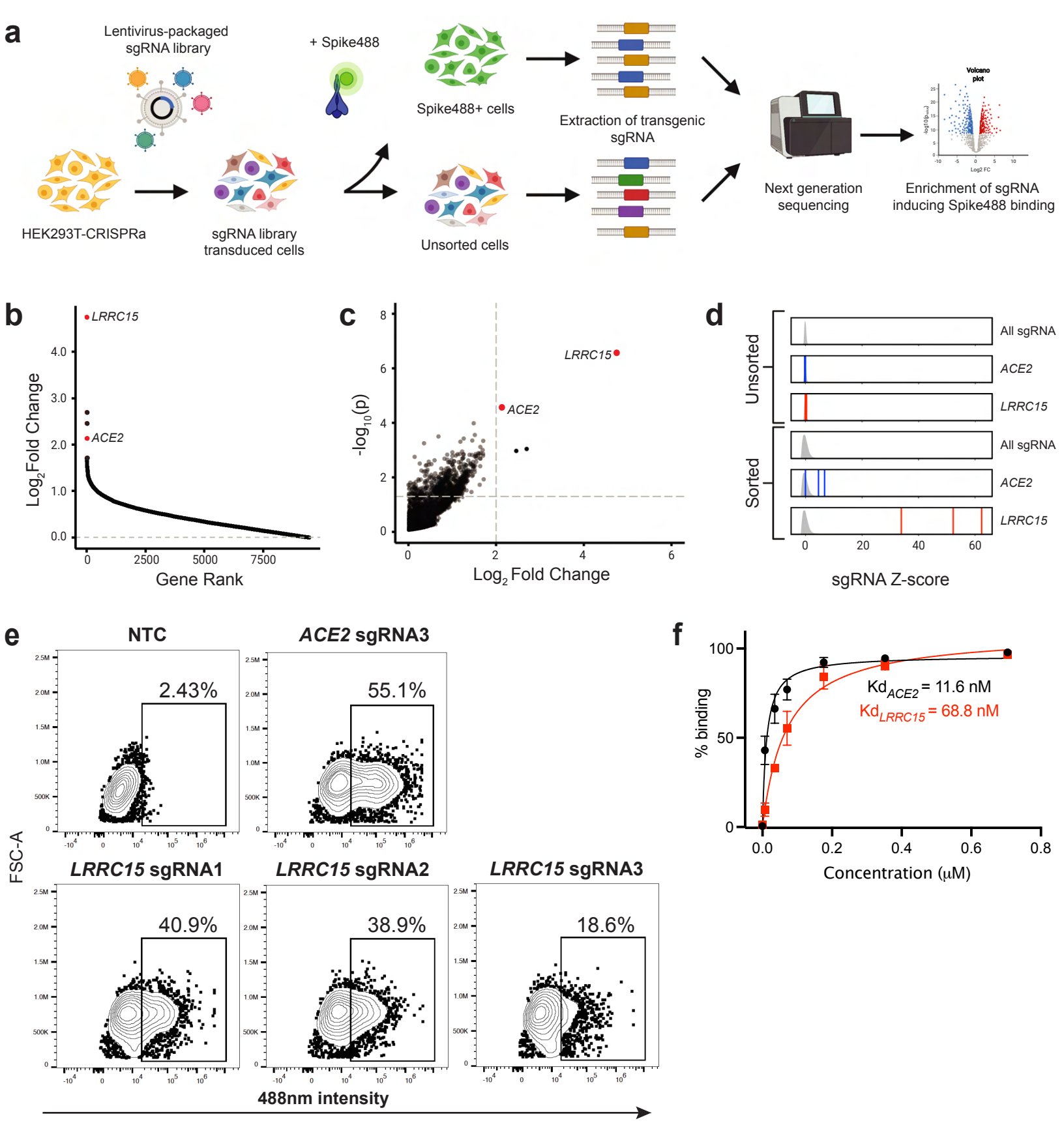
a
Lentivirus-packaged sgRNA library
+ Spike488
Spike488+ cells
Extraction of transgenic sgRNA
HEK293T-CRISPRa
sgRNA library transduced cells
Unsorted cells
Next generation sequencing
Volcano plot
Enrichment of sgRNA inducing Spike488 binding
b
LRRC15
ACE2
Log2 Fold Change
Gene Rank
c
LRRC15
ACE2
-log10(p)
Log2 Fold Change
d
Unsorted
Sorted
All sgRNA
ACE2
LRRC15
sgRNA Z-score
e
NTC
ACE2 sgRNA3
2.43%
55.1%
LRRC15 sgRNA1
LRRC15 sgRNA2
LRRC15 sgRNA3
40.9%
38.9%
18.6%
FSC-A
488nm intensity
f
% binding
Concentration (μM)
KdACE2 = 11.6 nM
KdLRRC15 = 68.8 nM

Figure 2

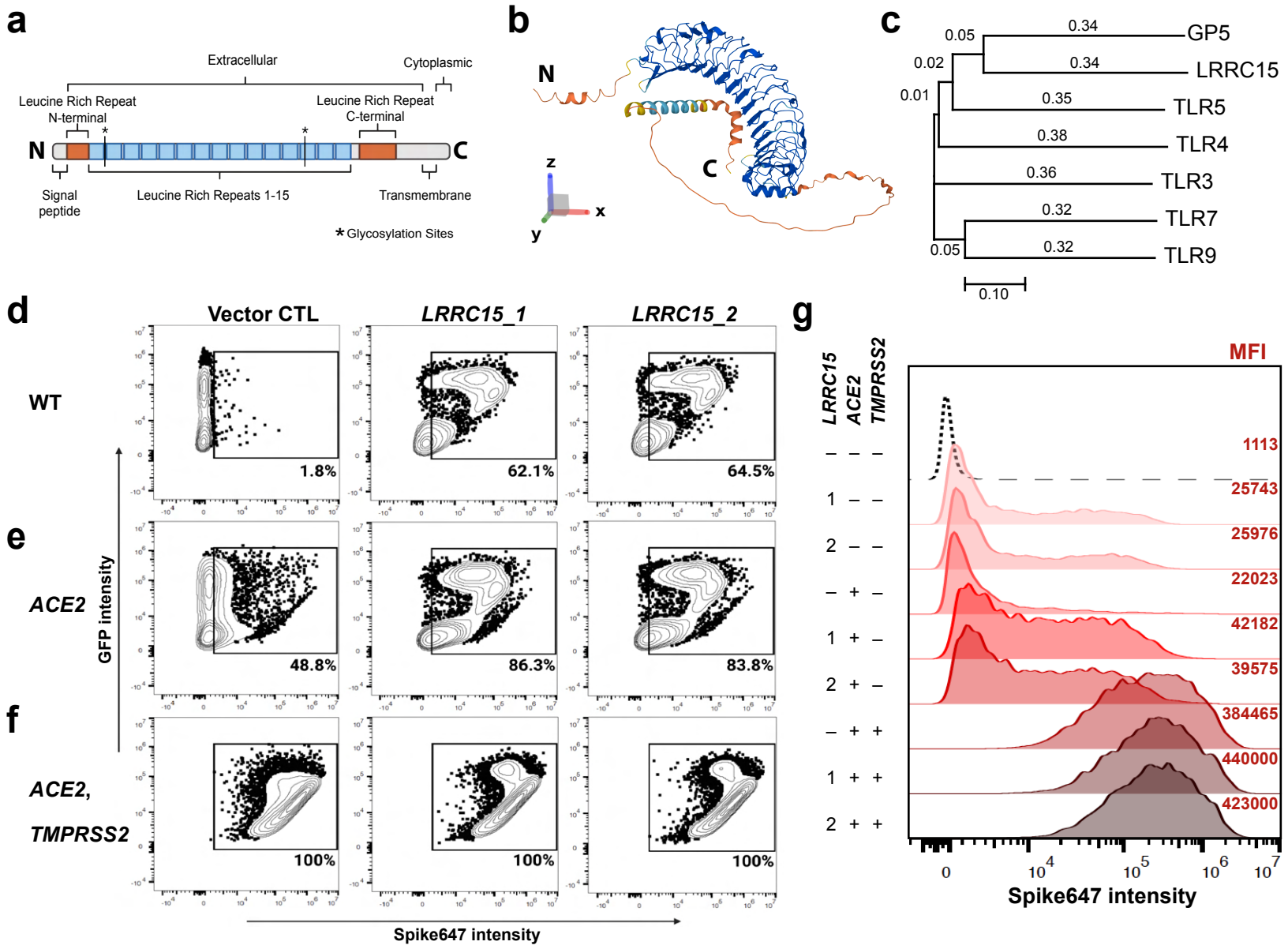
a
Extracellular
Cytoplasmic
Leucine Rich Repeat N-terminal
Leucine Rich Repeat C-terminal
N
C
Signal peptide
Leucine Rich Repeats 1-15
Transmembrane
* Glycosylation Sites
b
N
C
z
x
y
c
GP5
LRRC15
TLR5
TLR4
TLR3
TLR7
TLR9
0.05
0.34
0.02
0.34
0.01
0.35
0.38
0.36
0.32
0.05
0.32
0.10
d
Vector CTL
LRRC15_1
LRRC15_2
WT
1.8%
62.1%
64.5%
e
ACE2
48.8%
86.3%
83.8%
f
ACE2, TMPRSS2
100%
100%
100%
GFP intensity
Spike647 intensity
g
LRRC15
ACE2
TMPRSS2
MFI
1113
25743
25976
22023
42182
39575
384465
440000
423000
Spike647 intensity

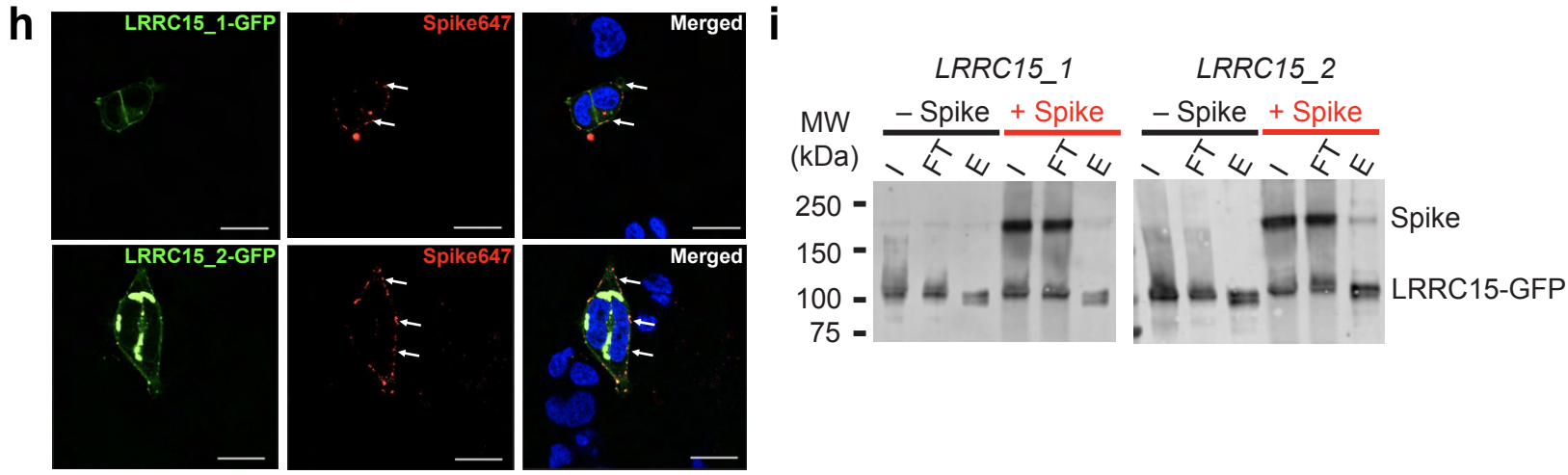
h
LRRC15_1-GFP
Spike647
Merged
LRRC15_2-GFP
Spike647
Merged
i
LRRC15_1
LRRC15_2
– Spike
+ Spike
– Spike
+ Spike
MW (kDa)
I
FT
E
250
150
100
75
Spike
LRRC15-GFP

Figure 3

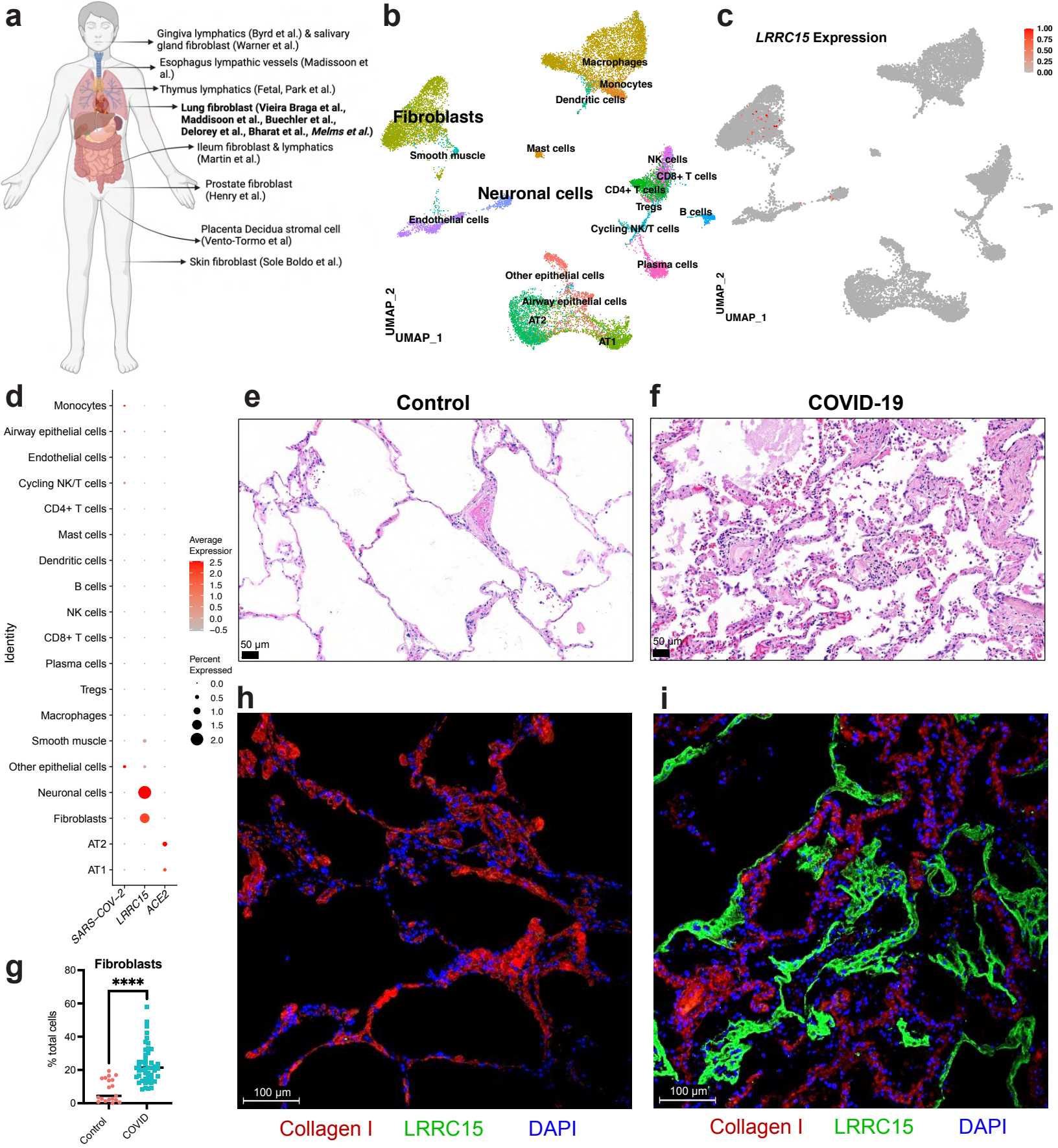
a
Gingiva lymphatics (Byrd et al.) & salivary gland fibroblast (Warner et al.)
Esophagus lympathic vessels (Madissoon et al.)
Thymus lymphatics (Fetal, Park et al.)
Lung fibroblast (Vieira Braga et al., Maddisoon et al., Buechler et al., Delorey et al., Bharat et al., Melms et al.)
Ileum fibroblast & lymphatics (Martin et al.)
Prostate fibroblast (Henry et al.)
Placenta Decidua stromal cell (Vento-Tormo et al)
Skin fibroblast (Sole Boldo et al.)
b
Macrophages
Monocytes
Dendritic cells
Fibroblasts
Smooth muscle
Mast cells
NK cells
CD8+ T cells
CD4+ T cells
Neuronal cells
Tregs
B cells
Endothelial cells
Cycling NK/T cells
Plasma cells
Other epithelial cells
Airway epithelial cells
AT2
AT1
UMAP_2
UMAP_1
c
LRRC15 Expression
1.00
0.75
0.50
0.25
0.00
UMAP_2
UMAP_1
d
Monocytes
Airway epithelial cells
Endothelial cells
Cycling NK/T cells
CD4+ T cells
Mast cells
Dendritic cells
B cells
NK cells
CD8+ T cells
Plasma cells
Tregs
Macrophages
Smooth muscle
Other epithelial cells
Neuronal cells
Fibroblasts
AT2
AT1
Identity
SARS-COV-2
LRRC15
ACE2
Average Expression
2.5
2.0
1.5
1.0
0.5
0.0
−0.5
Percent Expressed
0.0
0.5
1.0
1.5
2.0
e
Control
50 µm
f
COVID-19
50 µm
g
Fibroblasts
****
% total cells
80
60
40
20
0
Control
COVID
h
100 µm
Collagen I
LRRC15
DAPI
i
100 µm
Collagen I
LRRC15
DAPI

Figure 4

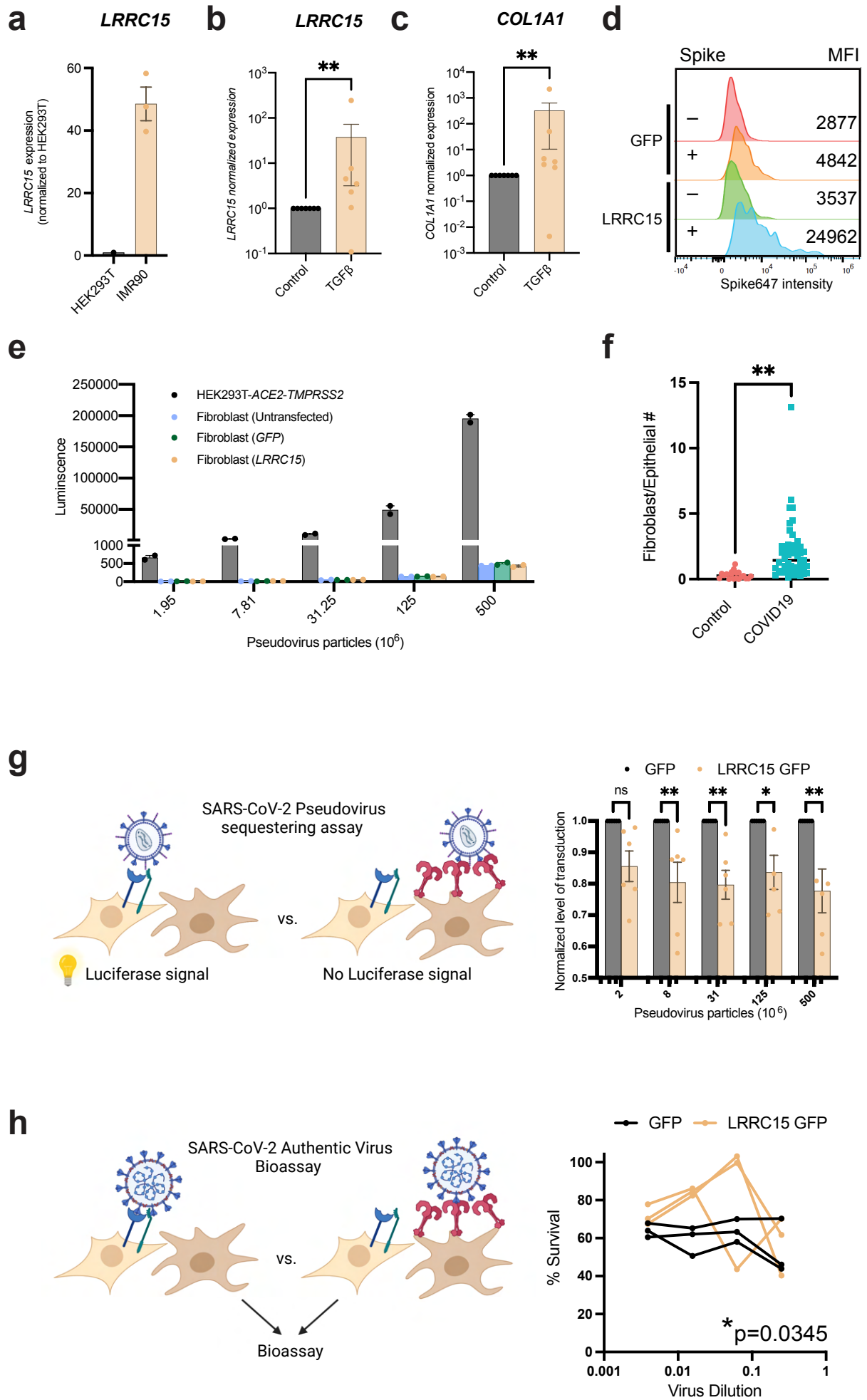
a
LRRC15
LRRC15 expression (normalized to HEK293T)
HEK293T
IMR90
b
LRRC15
LRRC15 normalized expression
Control
TGFβ
c
COL1A1
COL1A1 normalized expression
Control
TGFβ
d
Spike
MFI
GFP
LRRC15
2877
4842
3537
24962
Spike647 intensity
e
HEK293T-ACE2-TMPRSS2
Fibroblast (Untransfected)
Fibroblast (GFP)
Fibroblast (LRRC15)
Luminscence
Pseudovirus particles (10^6)
f
Fibroblast/Epithelial #
Control
COVID19
g
SARS-CoV-2 Pseudovirus sequestering assay
vs.
Luciferase signal
No Luciferase signal
GFP
LRRC15 GFP
Normalized level of transduction
Pseudovirus particles (10^6)
h
SARS-CoV-2 Authentic Virus Bioassay
vs.
Bioassay
GFP
LRRC15 GFP
% Survival
*p=0.0345
Virus Dilution

Figure 5

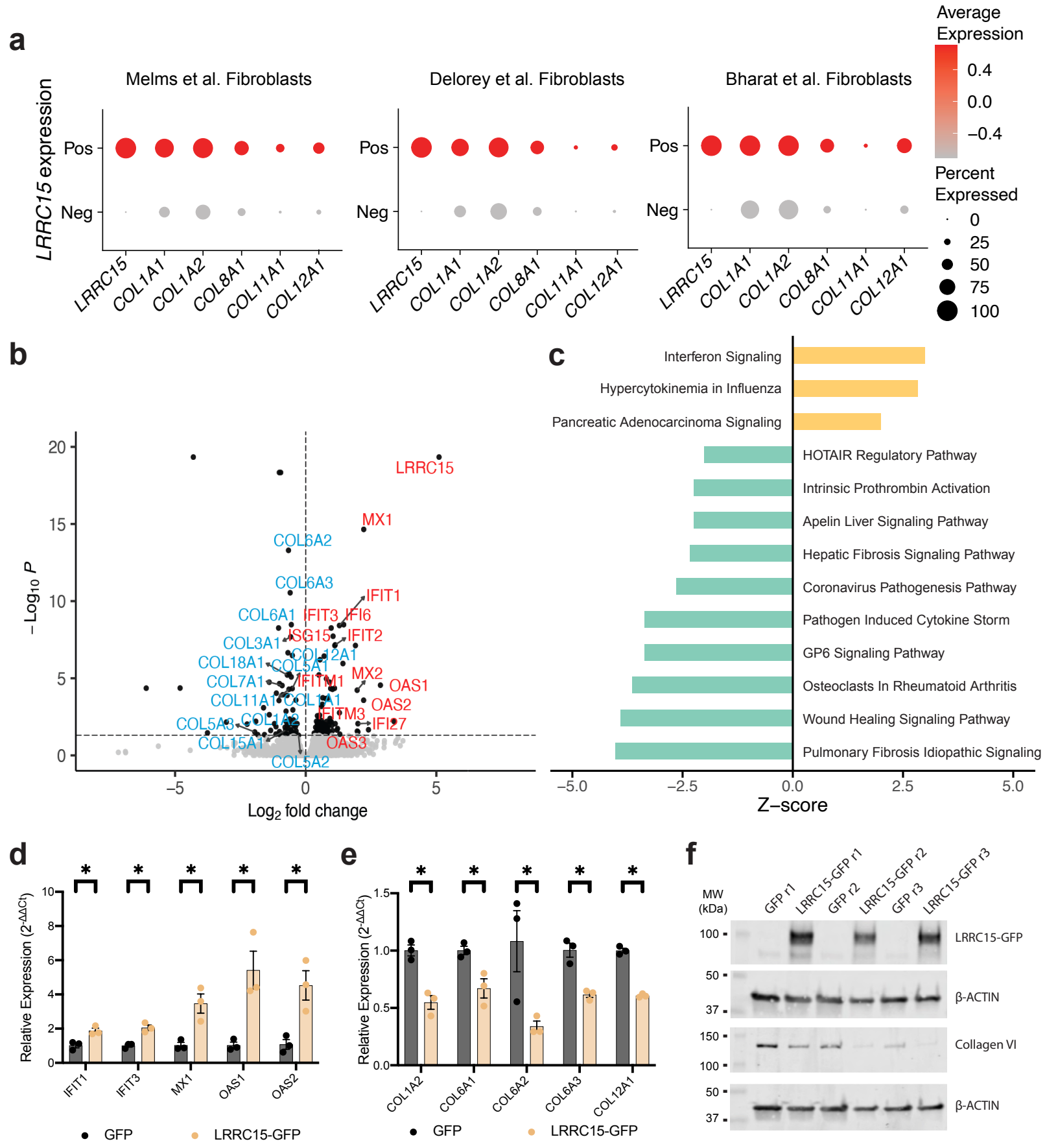
a
Melms et al. Fibroblasts
Delorey et al. Fibroblasts
Bharat et al. Fibroblasts
LRRC15 expression
Pos
Neg
LRRC15
COL1A1
COL1A2
COL8A1
COL11A1
COL12A1
Average Expression
0.4
0.0
−0.4
Percent Expressed
0
25
50
75
100
b
−Log10 P
Log2 fold change
LRRC15
MX1
COL6A2
COL6A3
IFIT1
COL6A1
IFIT3
IFI6
ISG15
IFIT2
COL3A1
COL12A1
COL18A1
COL5A1
MX2
COL7A1
IFITM1
OAS1
COL11A1
COL1A1
OAS2
COL5A3
COL1A2
IFITM3
IFI27
COL15A1
OAS3
COL5A2
c
Interferon Signaling
Hypercytokinemia in Influenza
Pancreatic Adenocarcinoma Signaling
HOTAIR Regulatory Pathway
Intrinsic Prothrombin Activation
Apelin Liver Signaling Pathway
Hepatic Fibrosis Signaling Pathway
Coronavirus Pathogenesis Pathway
Pathogen Induced Cytokine Storm
GP6 Signaling Pathway
Osteoclasts In Rheumatoid Arthritis
Wound Healing Signaling Pathway
Pulmonary Fibrosis Idiopathic Signaling
Z−score
d
Relative Expression (2-ΔΔCt)
IFIT1
IFIT3
MX1
OAS1
OAS2
GFP
LRRC15-GFP
e
Relative Expression (2-ΔΔCt)
COL1A2
COL6A1
COL6A2
COL6A3
COL12A1
GFP
LRRC15-GFP
f
MW (kDa)
GFP r1
LRRC15-GFP r1
GFP r2
LRRC15-GFP r2
GFP r3
LRRC15-GFP r3
LRRC15-GFP
β-ACTIN
Collagen VI
β-ACTIN

Figure 6

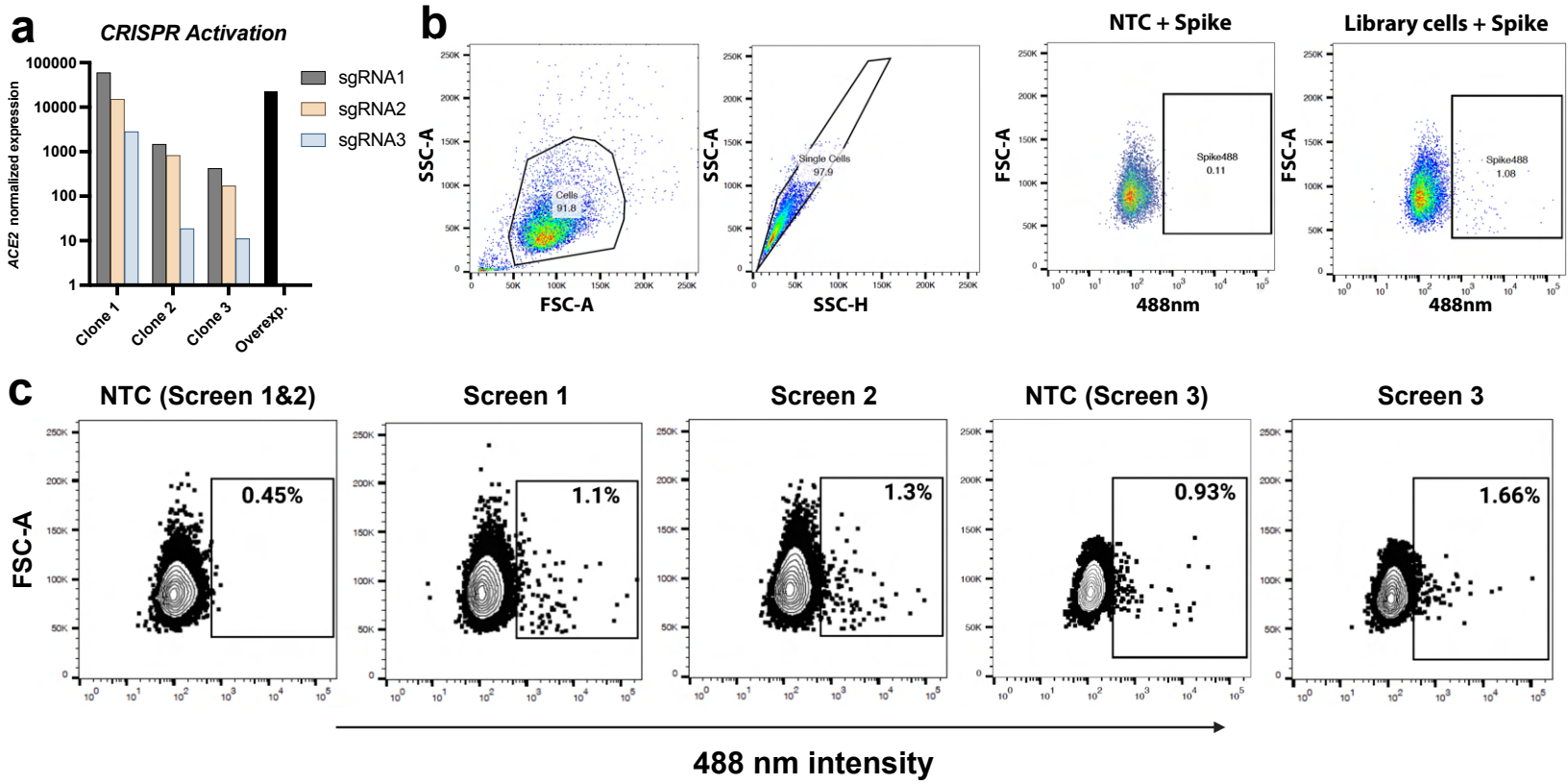

Supplementary Figure 1

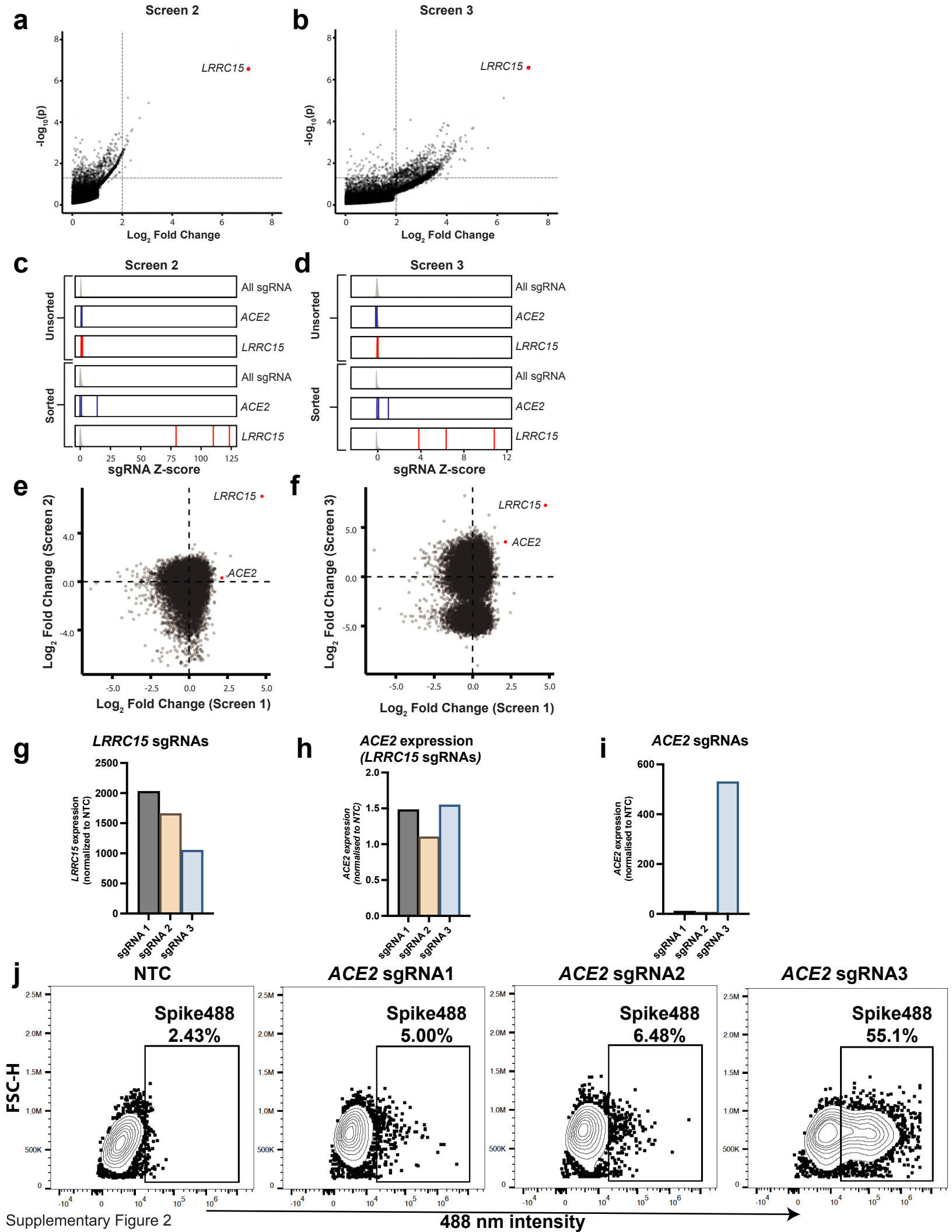

Supplementary Figure 2

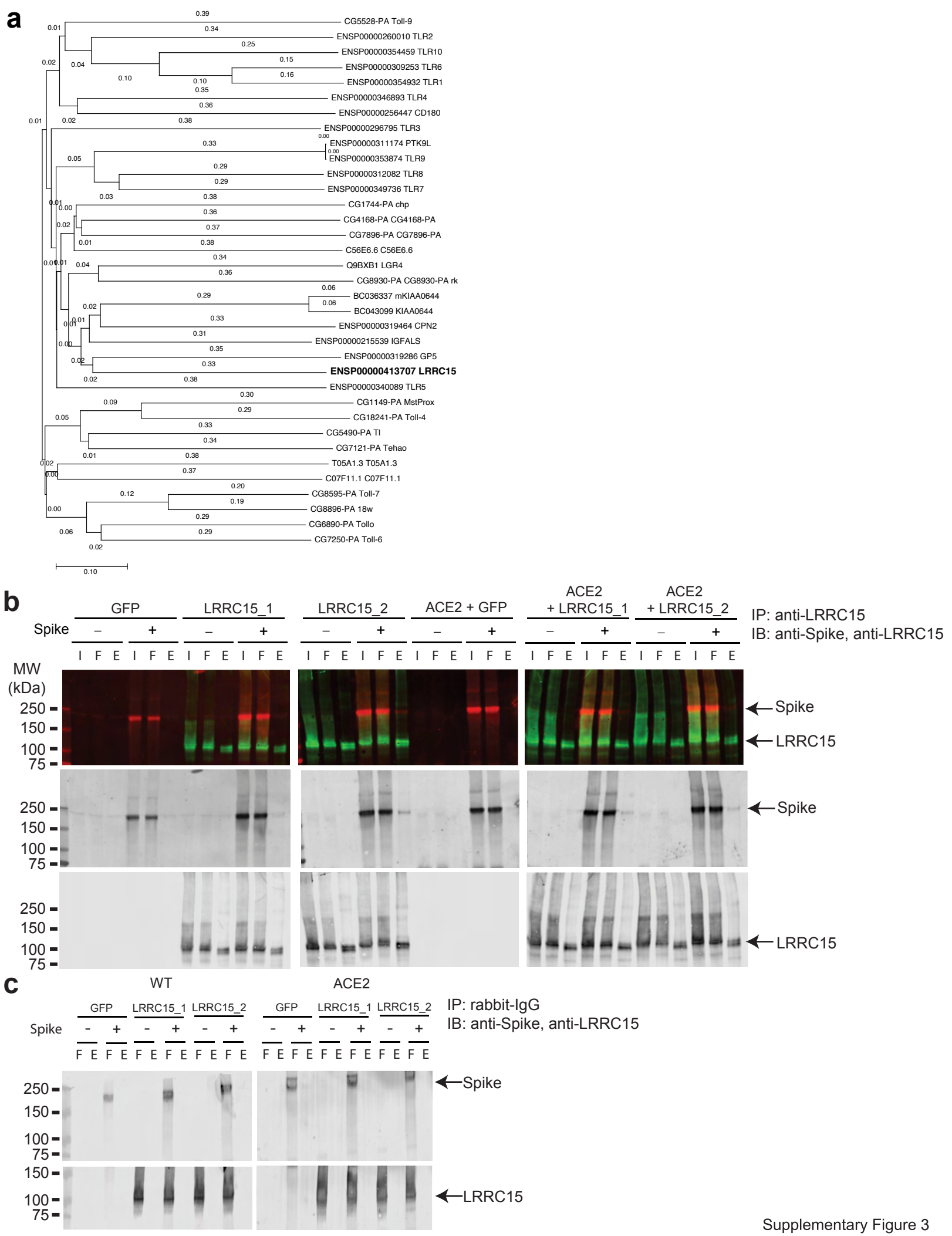

Supplementary Figure 3

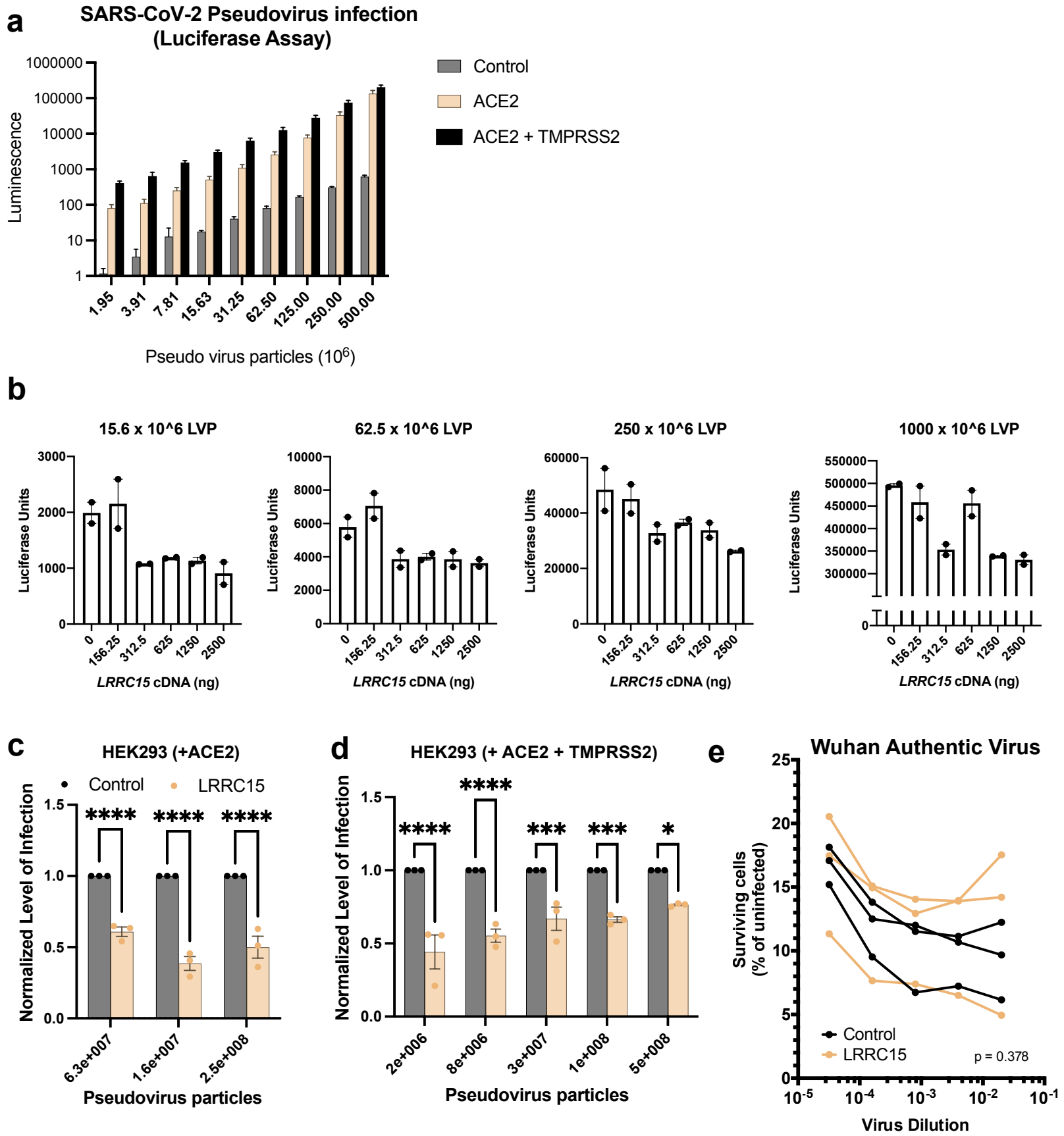

Supplementary Figure 4

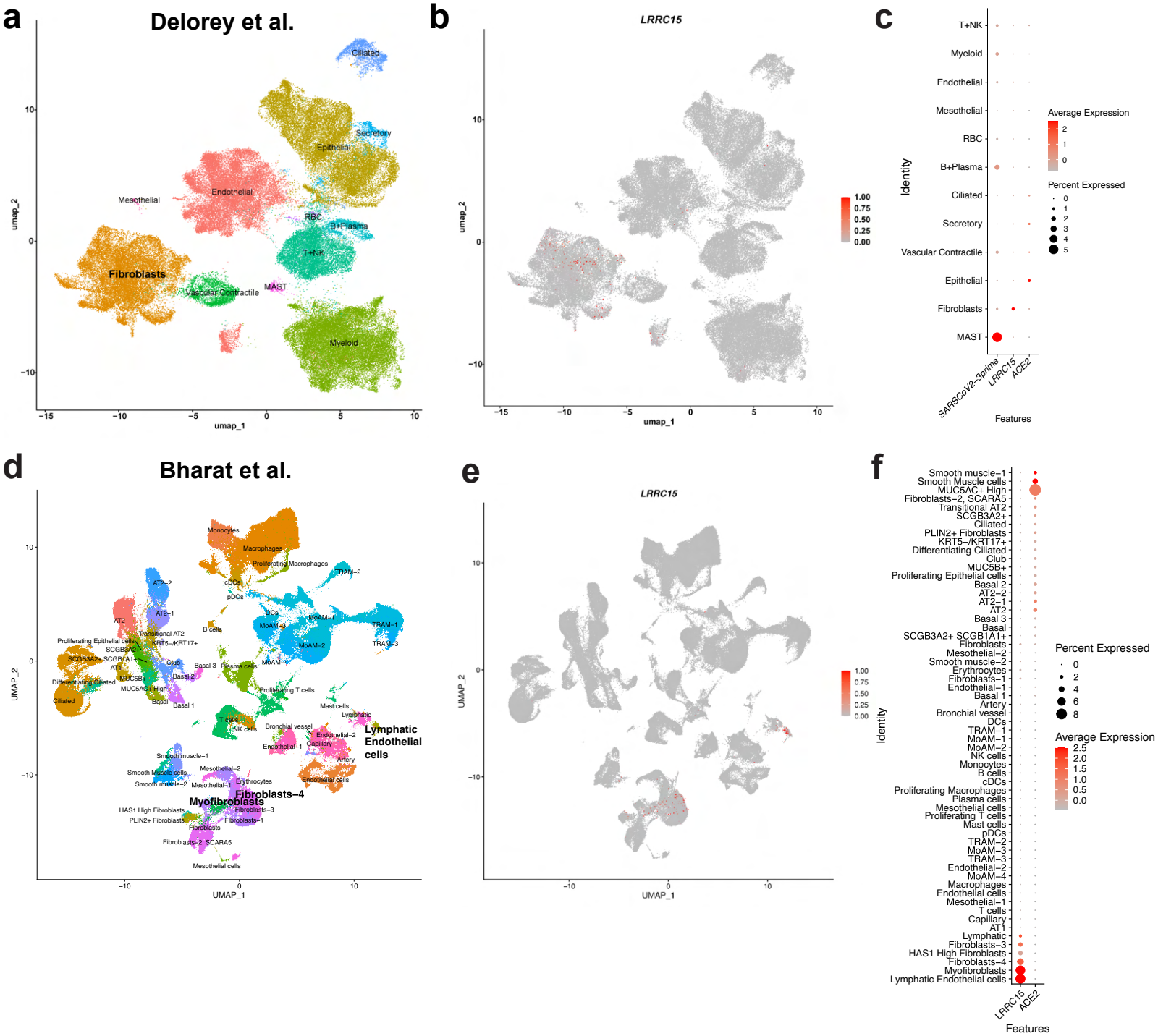

Supplementary Figure 5

a

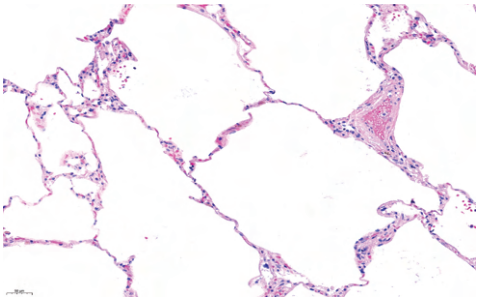

Control

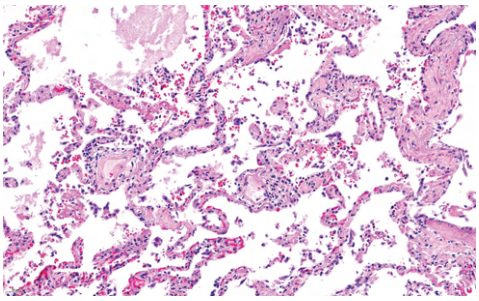

COVID 1

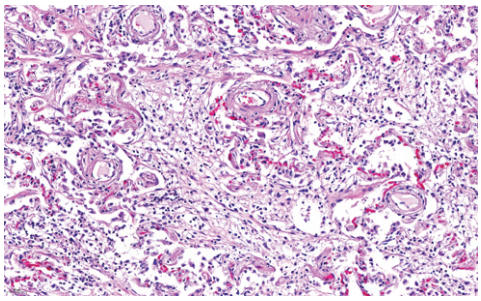

COVID 2

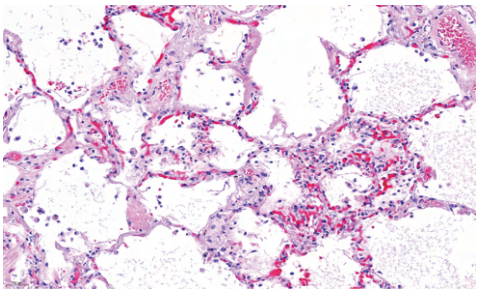

COVID 3

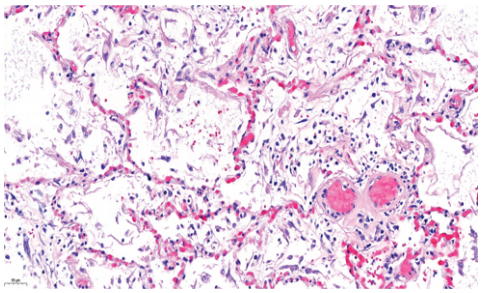

COVID 4

b

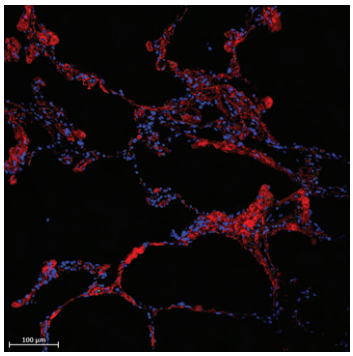

Control 1

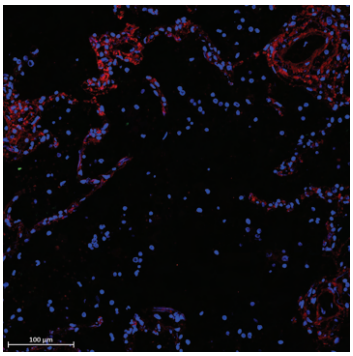

Control 2

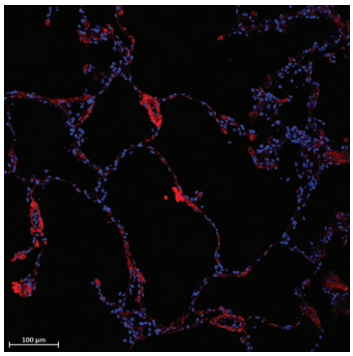

Control 3

Collagen I

LRRC15

DAPI

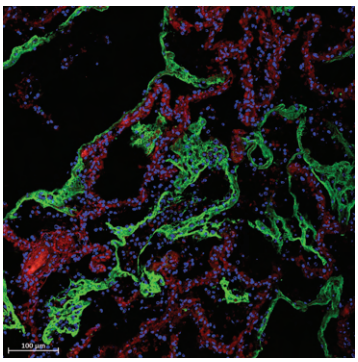

COVID 1

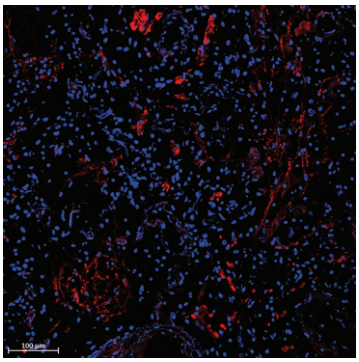

COVID 2

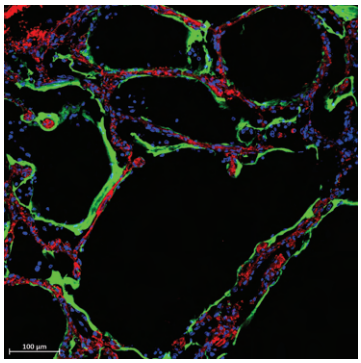

COVID 3

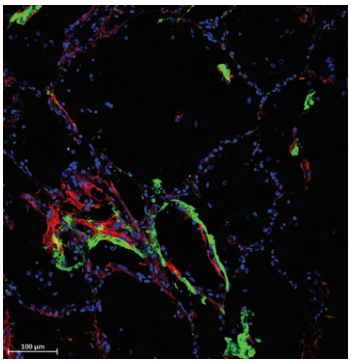

COVID 4

Supplementary Figure 6

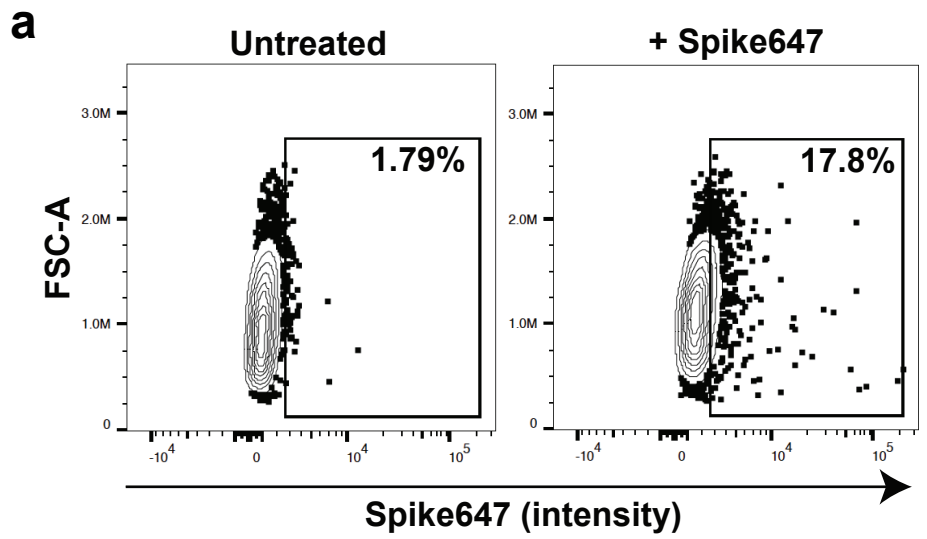

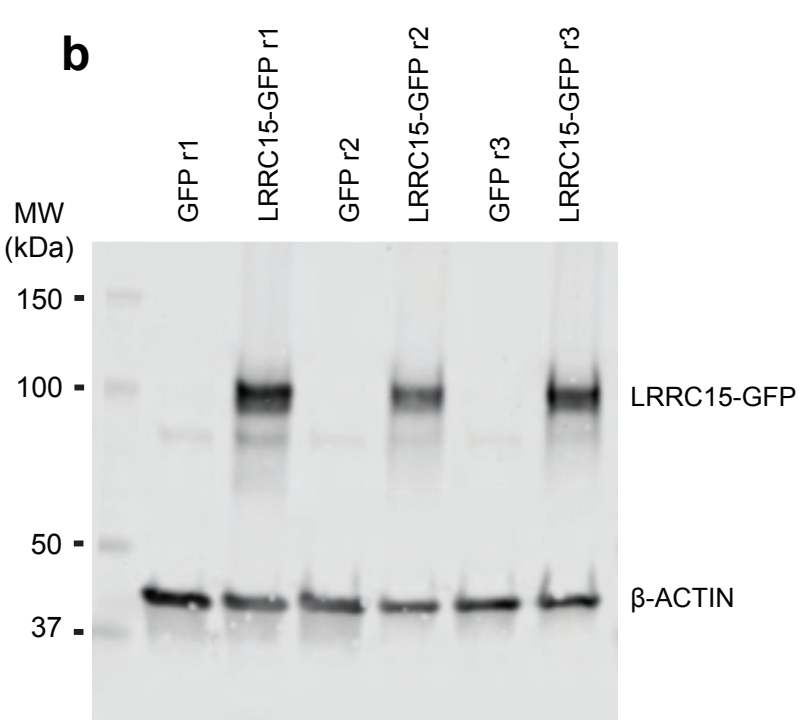

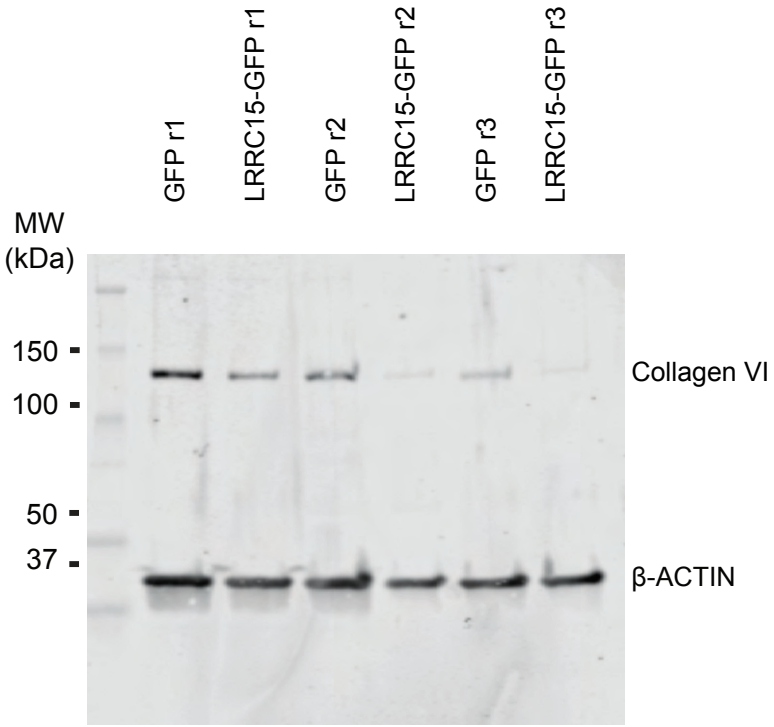

Supplementary Figure 7